CARDIFF UNIVERSITY
PRIFYSGOL CAERDYDD

ORCA – Online Research @ Cardiff

This is an Open Access document downloaded from ORCA, Cardiff University's institutional repository:https://orca.cardiff.ac.uk/id/eprint/112105/

This is the author's version of a work that was submitted to / accepted for publication.

Citation for final published version:

Pucilowska, Joanna, Vithayathil, Joseph, Pagani, Marco, Kelly, Caitlin, Karlo, J. Colleen, Robol, Camila, Morella, Ilaria , Gozzi, Alessandro, Brambilla, Riccardo and Landreth, Gary E. 2018. Pharmacological inhibition of ERK signaling rescues pathophysiology and behavioral phenotype associated with 16p11.2 chromosomal deletion in mice. Journal of Neuroscience 38 (30) , pp. 6640-6652. 10.1523/JNEUROSCI.0515-17.2018

Publishers page: http://dx.doi.org/10.1523/JNEUROSCI.0515-17.2018

Please note:
Changes made as a result of publishing processes such as copy-editing, formatting and page numbers may not be reflected in this version. For the definitive version of this publication, please refer to the published source. You are advised to consult the publisher's version if you wish to cite this paper.

This version is being made available in accordance with publisher policies. See http://orca.cf.ac.uk/policies.html for usage policies. Copyright and moral rights for publications made available in ORCA are retained by the copyright holders.

Title:

Pharmacological Inhibition of ERK Signaling Rescues Pathophysiology and Behavioral Phenotype Associated with 16p11.2 Chromosomal Deletion in Mice.

Abbreviated title:

Novel ERK inhibitor rescues deficits in a mouse model of autism.

Authors:

J. Pucilowska[1], J. Vithayathil[1], M. Pagani[2], C. Kelly[1], J. C. Karlo[1], C. Robol[2], I. Morella[3], A. Gozzi[2], R. Brambilla[3], and G.E. Landreth[1,4]

[1]Department of Neurosciences, Case Western Reserve University, Cleveland, Ohio 44106-4928

[2] Functional Neuroimaging Laboratory, Istituto Italiano di Tecnologia, Center for Neuroscience and Cognitive Systems @ UNITN Corso Bettini 31, 38068 Rovereto, Italy

[3] Neuroscience and Mental Health Research Institute and School of Biosciences, Cardiff University, Cardiff, UK.

[4] Stark Neuroscience Research Institute, Indiana University School of Medicine, Indianapolis, IN 46202

Corresponding Author:

Dr. Gary Landreth
Stark Neuroscience Research Institute
Indiana University School of Medicine
320 W. 15th St., NB214C
Indianapolis, IN 46202
317 278 7820- office
Email: glandret@iu.edu

Number of pages: 38

Number of figures: 7

Number of words: Abstract (143), Significance Statement (120), Introduction (585), Discussion(1484)

Conflict of Interest: The authors declare no competing financial interests.

Acknowledgements: This work was supported by grants from the Simons Foundation (SFARI 275316, GEL). A. Gozzi acknowledges funding from the Simon Foundation (SFARI 314688 and 400101, AG) and the Brain and Behavior Foundation (NARSAD, AG). I. Morella acknowledges support from the Waterloo Foundation.

Abstract:

The human *16p11.2* microdeletion is one of the most common gene copy number variations linked to autism, but the pathophysiology associated with this chromosomal abnormality is largely unknown. The 593-kb deletion contains the ERK1 gene and other genes that converge onto the ERK/MAP kinase pathway. Perturbations in ERK signaling are linked to a group of related neurodevelopmental disorders hallmarked by intellectual disability, including autism. We report that mice harboring the *16p11.2* deletion exhibit a paradoxical elevation of ERK activity, cortical cytoarchitecture abnormalities and behavioral deficits. Importantly, we show that treatment with a novel ERK pathway inhibitor during a critical period of brain development rescues the molecular, anatomical and behavioral deficits in the *16p11.2* deletion mice. The ERK inhibitor treatment administered to adult mice ameliorates a subset of these behavioral deficits. Our findings provide evidence for potential targeted therapeutic intervention in *16p11.2* deletion carriers.

Significance Statement:

The ERK/MAPK pathway is genetically linked to autism spectrum disorders and other syndromes typified by intellectual disability. We provide direct evidence connecting the ERK/ MAP kinases to the developmental abnormalities in neurogenesis and cortical cytoarchitecture associated with the *16p11.2* chromosomal deletion. Most importantly, we demonstrate that treatment with a novel ERK specific inhibitor during development rescues aberrant cortical cytoarchitecture and restores normal levels of cell cycle regulators during cortical neurogenesis. These treatments partially reverse the behavioral deficits observed in the *16p11.2del* mouse model, including hyperactivity, memory as well as olfaction, and maternal behavior. We also report a rescue of a subset of these deficits upon treatment of adult *16p11.2del* mice. These data

provide a strong rationale for therapeutic approaches to this disorder.

Introduction:

Autism Spectrum Disorders (ASDs) are complex, highly heritable neurodevelopmental disorders affecting approximately 1 in 100 children. Copy number variations (CNVs) and other chromosomal rearrangements are associated with approximately 10-20% of ASDs. CNV of human chromosome *16p11.2* is one of the most common genetic linkages to autism and deletion of this region accounts for approximately 1% of ASDs (Levy et al., 2011). Individuals heterozygous for the *16p11.2* deletion exhibit a range of clinical symptoms including ASD, language impairment, intellectual disability (ID), anxiety, attention deficit hyperactivity disorder and epilepsy (Ghebranious et al., 2007; Zufferey et al., 2012; Hanson et al., 2015a). The human *16p11.2* locus contains 27 genes, which includes the *MAPK3* gene (encoding ERK1) and the Major Vault Protein gene (*MVP*), both of which converge onto the ERK/MAP kinase pathway (Kumar et al., 2007).

The extracellular signal-regulated kinases, ERK1 and ERK2, are central elements of one of the most prominent intracellular signaling cascades, the Mitogen Activated Protein Kinase (MAPK) pathway. The ERKs play critical roles in brain development and synaptic plasticity (Sweatt, 2004) and are activated in response to a broad range of stimuli including growth factors, neurotransmitters, morphogens and transient increases in synaptic Ca2+ (Roskoski, 2012). Importantly, they are genetically linked to ASDs and other syndromes typified by ID (Marshall et al., 2008; Wen et al., 2016; Borrie et al., 2017; Mitra et al., 2017). Mutations in elements of the ERK/MAPK pathway alter the activity of the ERKs, resulting in a group of genetic disorders collectively known as “RASopathies”. These syndromes are typified by ID, developmental and language deficits, ASD and psychiatric disease (Tidyman and Rauen, 2009; Fasano and

100 Brambilla, 2011).

101 We have previously reported that a murine model of the *16p11.2* human microdeletion
102 *(16p11.2del*) exhibits a reduction in brain size and perturbations in cortical
103 cytoarchitecture,which are postulated to be due to impaired ERK-mediated regulation of neural
104 progenitor proliferation (Newbern et al., 2008; Pucilowska et al., 2015). The *16p11.2del* mice
105 exhibit a paradoxical increase in ERK signaling coincident with aberrant cortical neurogenesis,
106 ultimately resulting in behavioral deficits analogous to the *16p11.2* microdeletion carriers
107 (Portmann et al., 2014; Hanson et al., 2015b). Therefore, we postulated that treatment with brain
108 permeable Ras-ERK pathway inhibitors may correct the pathophysiology associated with the
109 *16p11.2* deletion. Recently, we have validated two novel cell permeable peptides (CPPs), RB1
110 and RB3, that efficiently inhibit Ras-ERK signaling in the post-natal developing brain and rescue
111 morphological impairments in a severe mouse model of RASopathies (Papale et al., 2017). In
112 addition, the RB1 and RB3 peptides are able to block cocaine-mediated ERK activation and the
113 associated behavioral response (Papale et al., 2016).

114 In this study, we report that prenatal treatment with cell permeant RB1/RB3 peptides
115 rescues developmental deficits in neurogenesis in the embryo and subsequently restores normal
116 neuronal numbers and cortical cytoarchitecture in the *16p11.2del* mice. Specifically, we report
117 restoration of hippocampal based memory function, anxiety, olfaction, maternal behavior as well
118 as hyperactivity in the 16p11.2del mice. Furthermore, postnatal drug treatment of adult
119 *16p11.2del* mice results in partial amelioration of the behavioral deficits, suggesting a broader
120 window for pharmacologic intervention. To assess the macroscale anatomical substrates affected
121 by the drug treatment, we used high-resolution morphoanatomical MRI mapping to show partial
122 restoration of gray matter volume in ventral hippocampal and lateral septal regions, which we

found to be reduced in the *16p11.2del* mice. We conclude that treatment with ERK pathway inhibitors may represent a potential therapeutic intervention in *16p11.2del* carriers, as has been suggested for RASopathies (Tidyman and Rauen, 2009). This is the first example of the rescue of development abnormalities in this ASD model.

Materials and Methods:

Animals. A mouse line carrying a microdeletion on chromosome *7qF3*, the syntenic region of human chromosome *16p11.2*, was generated by A. Mills and purchased from Jackson Labs (Horev et al., 2011). This mouse line has been maintained on a fixed ratio, mixed (129/C57) background with large numbers of mice examined to minimize any genetic background-associated variation. Embryonic and adult treatments were 5 days long and administered by sub-cutaneous injections of ERK inhibitor resuspended in PBS at a dose of 10mg/kg. Pregnant dams were used with a plug date designated as 0.5 days.

Drugs: RB1 and RB3 cell permeable peptides have been recently described (Papale et al., 2016). Briefly, RB1 was designed around residues 59-73 within the KIM sequence of the ERK-specific phosphatase MKP3 (Liu et al., 2006) that interacts with a docking motif required for interactions of ERK1/2 with both its regulators and substrates. RB3 was designed, using the MOE software package, (Molecular Operating Environment, version 10.10, Chemical Computing group, Montreal Canada, http://www.chemcomp.com) by aligning and superposing the CDC25 domain of Ras-GRF1 (Freedman et al., 2006) the published crystal structure of a ternary Ras:SOS:Ras*GDP complex (Sondermann et al., 2004) using the default settings. The interacting surface between the two proteins was then visually analyzed and the portion of the

CDC25 domain between residues 1173 to 1203 was selected for the preparation of the final peptide. RB1 (MGRKKRRQRRRPPQAPGIMLRRLQKGNLPVSRYPYDVPD), SCR RB1 (MGRKKRRQRRRPPQALSLKRLRSRGMNRTSATQSRYPYD), RB3 (GRKKRRQRRRPPCVPYLGMYLTDLVFIEEGTPNYTEDGLVN) and SCR RB3 (GRKKRRQRRRPPCFEVYPDSGDYTYEGELNGTLMVVPTN) were custom synthesized by GENECUST EUROPE (Luxembourg).

For *in vivo* experiments, batches of 200 mg, highly purified by high-performance liquid chromatography (HPLC) (≥ 95 %) with C-terminal amino acid (last) in D form and acetylated N-Terminal (first) amino acid were used. The peptides were dissolved in PBS 1X and injected 10 mg/kg (i.p.) (10 mg/kg each peptide) intraperitoneally.

Sample preparation and MRI acquisition: High-resolution morpho-anatomical T2-weighted MR imaging of P90 *ex vivo* mouse brains was performed in paraformaldehyde fixed specimens. Standard sample preparation and MRI acquisition have been recently described in detail (Cutuli et al., 2016). Briefly, *16p11.2del* mice and age-matched control littermates (treated with ERK inhibitor or vehicles) were deeply anesthetized and their brains were perfused *in situ* via cardiac perfusion. The perfusion was performed with phosphate buffered saline followed by paraformaldehyde (4% PFA; 100 ml). Both perfusion solutions included a gadolinium chelate (Prohance, Bracco, Milan) at a concentration of 10 and 5 mM, respectively, to shorten longitudinal relaxation times. Brains were imaged inside intact skulls to avoid post-extraction deformations. A multi-channel 7.0 Tesla MRI scanner (Bruker Biospin, Milan) was used to acquire anatomical images of the brain, using a 72 mm birdcage transmit coil and a custom-built saddle-shaped solenoid coil for signal reception, with the following imaging parameters: FLASH

3D sequence with TR = 17 ms, TE = 10 ms, alpha = 30°, matrix size of 260 × 180 × 180, field of view of 1.82 × 1.26 × 1.26 cm and voxel size of 0.07 mm (isotropic).

Tensor Based Morphometry (TBM) automated anatomical labeling and structural covariance MRI network mapping. Inter-group morpho-anatomical differences in local volumes were mapped with TBM (Ashburner & Friston, 2000) using ANTs (Avants et al., 2009). The registration-based TBM procedure employed has been thoroughly described elsewhere (Pagani et al., 2016). First, all the high-resolution T2-weighted images were corrected for intensity non-uniformity and skull stripped to remove extra-brain tissue. A study-based template was then created aligning pre-processed images to a common reference space using affine and diffeomorphic registrations. Individual images of *16p11.2del* and control mice (treated with ERK inhibitor or vehicle) were registered to the study-based template and the Jacobian determinants of the deformation fields were calculated at each voxel, giving the voxel's relative expansion or contraction in the space of the study-based template. Jacobian determinants were also normalized by the total intracranial volume to further eliminate overall brain volume variations. We measured non-normalized intracranial brain volume in all the four treatment groups at P90 . The results we obtained showed the presence of smaller brain volume in 16p11.2 mutants, a finding previously reported in mice modelling 16p11.2 deletion (Portmann et al., 2014). The treatment did not affect total intracranial volume in either WT or *16p11.2* mutants. The resulting maps were smoothed using a Gaussian kernel with a sigma of three voxel width and employed for voxel-wise statistics. Regional volume differences between *16p11.2del* and control mice were mapped by fitting a GLM ($t > 2.3$) followed by a cluster correction using a significant cluster threshold of $p = 0.01$ (Worsley et al., 1992) as implemented in FSL. We also employed preprocessed images to independently calculate volumes of brain regions via automated

anatomical labeling (Pagani et al., 2016), using two neuroanatomically parcellated reference MRI atlases for cortical (Ullmann et al., 2013) and subcortical areas (Dorr et al., 2008).

Behavioral analysis. Three-month-old male and female mice were utilized for standardized behavioral analyses including the elevated plus maze, open-field, novel object recognition, olfaction, maternal behavior and fear conditioning tests in order as stated. All tests were conducted in a designated behavior room during the light cycle between 9:00 A.M. and 6:00 P.M. A maximum of 5 mice of mixed genotypes were housed together with ad libitum access to food and water with a 12 h light/dark cycle. All equipment was cleaned with 70% ethanol after each use to remove odor cues. The tester was blinded to the genotype of each animal. All tests were performed at the Case Western Reserve University Rodent Behavior Core. Three different cohorts (each with at least 50 mice divided to include both genotypes and treatment paradigms) were evaluated in three independent experiments. The data represents the pooled analysis of all three cohorts.

The elevated plus maze: The maze consisted of two open and two closed arms crossing each other approximately 1 m above the floor. The maze was fitted with infrared grid and video tracking system (Med Associates Inc.). Individual test mice were placed in the center facing the open arm and their activity was recorded for 5 minutes. The % time spent in open and closed arms, the number of entries into each arm, number of head dips and frequency of urination/defecation were scored.

Open field test: A box (40cm x 40cm) was placed in a dimly lit environment. EthoVision XT 5.0 (Noldus) was used to digitally subdivide the box area into a 20 cm Å~ 20 cm center area and a periphery. The peripheral area was further divided into middle (inner 10 cm) and an outer area (outer 10 cm) to determine thigmotaxic behavior. Mice were placed in the center and allowed to

explore the area freely for 15 min. Locomotion parameters such as total distance, velocity, angular velocity and immobility were measured. Frequency and time duration in the center, periphery and outer area were recorded to determine anxiety-like behavior. In addition, data were nested into 5-min bins and distance moved during each of these 3 periods was recorded to evaluate habituation differences across groups.

Novel Object: This assay was conducted 24 hours following the open field test in the same arena. Each subject mouse was placed in the chamber containing two identical objects and allowed free exploration for 10 minutes. Following a 3 hour delay, one of the familiar objects was replaced with a novel object and the test mice were returned to the same arena. The time spent sniffing each object was measured. Tester was blinded to the genotypes of tested mice. We scored and reported raw data of time spend sniffing novel (NO) vs. habituated object (HO) Mice that did not sniff either object and/or did not sniff for a total of 4 seconds were excluded from the final analysis.

Olfactory Assay: Buried Food Retrieval. Mice were food deprived overnight and places in standard clean cages with normal cage bedding (3 cm). Mice were allowed to acclimate for 5 minutes, then were removed to another clean cage at which point a uniform piece of food (Teddy Graham) was placed in a random corner under approximately 1cm of normal bedding. Next, each mouse was returned to its cage and the time to retrieve the food source (latency) was recorded.

Contexual and Cued Fear Conditioning: Fear conditioning test was conducted as the last behavioral test in the series of all behavioral assesments. Experiments utilized two standard conditioning chambers, each housed in an isolation cubicle and equipped with a stainless-steel grid floor connected to a solid-state shock scrambler. Each scrambler delivered an electronic constant-current shock source that was controlled via an interface connected to a Windows XP

computer running FreezeFrame software (Coulbourn Instruments, Allentown, PA). A digital camera was mounted to the side of each chamber, and video signals were sent to the same computer for analysis. During training, mice were placed in the conditioning chamber for 12 min and then received four footshocks (cond. stimulus: 85 dB sound at 2800 Hz for 30 sec.; unconditioned stimulus (US: 0.56mA). Retention test was performed 18 hrs later for 5 minutes in the absence of a shock.

Analysis of progenitor proliferation. Mice received a single intraperitoneal injection of BrdU (50 mg/kg, Sigma-Aldrich B5002) at E14.5 and sacrificed exactly 30 minutes later (veh.treated: n_{WT} = 8, n_{Del}=6; inh.treated: n_{WT} = 9, n_{Del}=9). Sections were immunostained with anti-BrdU antibody, (rat-anti-BrdU; 1:100, Abcam), or mouse anti-BrdU (1:100, BD Biosciences). The number of BrdU+ cells per cortical sections (proliferative fraction) was established using stereological technique and all positive cells within a 100µm segment along the ventricular surface, extending from the ventricle to the pial surface, were counted. All data collection was blinded to the genotype and randomized. In embryonic brains all analyses were performed at the rostro-caudal axis of fully emerged ganglionic eminences, (LGE as well as MGE). These structures as well as the presence of choroid plexus were noted and the images were taken just above the pallial/subpallial boundary in the VZ as well dorso-medial area of the VZ. In adult mice we evaluated BrdU staining in two different areas; 1) above the pallial/subpallial boundary (dorsolateral), the other (2) at the level of dorsomedial cortex. For postnatal analyses we evaluated both motor and somatosensory cortex.

Microscopy and image analysis. All sections were imaged using a Zeiss LSM 510 confocal laser microscope equipped with argon and helium–neon lasers and analyzed with LCS confocal software, Prism and Photoshop (Adobe). All counts were performed on blinded sections and

two-way ANOVA with Bonferroni post hoc was used to establish statistical significance for each experiment.

Western analysis. Cortices were dissected from E14.5 embryos and washed with ice-cold HBSS. The lysates were sonicated in lysis buffer (20 mM Tris, pH 7.5,150 mM NaCl, 1% NP-40, 10% glycerol, 1 mM EDTA, 1.5 mM $MgCl_2$, 20 mM NaF, and 20 mM -glycerophosphate) in the presence of protease inhibitors (1 g/ml leupeptin, 1 g/ml aprotinin, 1 mM PMSF, and 1 mM Na_3VO_4). Samples were centrifuged, and protein concentrations were established with bicinchoninic acid assay (Pierce) using a BSA standard. Equal amounts of protein were boiled in sample buffer, separated on SDS-PAGE gels, and transferred to Immobilon-P polyvinylidene difluoride membranes (Millipore). Membranes were blocked in 3% BSA (or 5% skim-milk) in TBS and 0.1% Tween 20 (TBS-T) for 2 h at room temperature and incubated with primary antibodies overnight at 4°C. The primary antibodies used were: rabbit anti-pERK (Cell Signaling, 1:1000), mouse anti-ERK2 (BD Biosciences Discovery Labware, 1:3000), mouse anti-ERK1 (Zymed Laboratories, 1:1000), anti-CoxIV and (1:3000; Cell Signaling). Membranes were washed with TBS-T, incubated with HRP-conjugated secondary antibodies: goat anti-mouse or anti-rabbit (1:5000; GE Healthcare) in TBS-T with 5% milk for 2 h at room temperature. Detection was performed using Millipore chemiluminescence using BioMax MR X-ray film (Eastman Kodak). Densitometry was performed using Adobe Photoshop histogram function, and statistical analysis was done with GraphPad Prism software.

ELISA. The oxytocin (OT) Elisa was performed using ENZO Oxytocin kit (Prod.No. ADI-901-153A) according to the manufactures instructions. Whole brain homogenates of P90 WT and *16p11.2del* brains were used and the calometric readout was reported in pg/ml.

Immunohistochemistry. The E14.5 brains were dissected in cold PBS and fixed by immersion

283 in 4% paraformaldehyde (PFA) for 1hour or overnight at 4° C. P10 and adult mouse brains were
284 fixed in 4% PFA/1X PBS at 4°C overnight and serially incubated in 10, 20 and 30% sucrose.
285 The brains were sectioned (10 m), then rehydrated in PBS for 10 min. Antigen retrieval using
286 1X Reveal Decloaker (Biocare) was performed for 10 minutes at 95°C. Sections were blocked in
287 10% (embryonic) and 2% (postnatal) normal goat or donkey serum for 1 hour at room
288 temperature with 0.1% (vol/vol) Triton X-100 in PBS. Slides were incubated with primary
289 antibodies overnight at 4°C, rinsed with PBS and incubated with corresponding secondary
290 antibodies for 1-2 hours at room temperature. The primary antibodies used were as follows:
291 polyclonal rabbit anti-pERK (Cell Signaling, 1:100); rabbit polyclonal anti-Pax6 (Covance,
292 1:300); mouse anti-PH3 (Upstate, 1:250); rabbit anti-PH3 (Upstate, 1;500); rabbit anti-Tbr1
293 (Chemicon,1:1000); rabbit anti-Tbr2 (1:300); chicken anti-Tbr2 (1:250); goat anti-Brn1 (Santa
294 Cruz Biotechnology, 1:50), rat anti-Ctip2 (Abcam,1:500); rabbit anti-Cux1 (Santa Cruz, 1:100)
295 and mouse anti-SatB2 (Abcam, 1:100). Secondary antibodies used were Alexa Fluor 488
296 (1:1000), 546 or 593 (1:1000) conjugated to goat or donkey anti-mouse, anti-rabbit or anti-goat
297 (Invitrogen). DNA was stained with 4 ,6 -diamidino-2-phenylindole (DAPI) for 5 min
298 (DAPI, Molecular Probes). Immunohistochemical staining was performed on all 4 groups
299 simultaneously.
300 ***Embryonic Brains.*** Anatomically matched sections of littermate WT and mutant mice were
301 analyzed. At least 3 consecutive sections per animal were analyzed alongside the mid-rostro-
302 caudal axis of the dorsal telencephalon. Embryonic coronal sections were evaluated at the level
303 of the ganglionic eminences and analyzed by counting all cells in standard 100μm bins extending
304 from the ventricle to the pial surface. Quantification was performed blind to genotype as
305 previously described (Glickstein et al., 2009). Three to four litters were examined per

306 experiment.

307 ***Adult Brains***. We counted at least three consecutive tissue slices per slide and at least four slides
308 per animal. In postnatal brains, coronal sections were used to count cells in 400 m boxes in
309 somatosensory and motor cortex. Slides were picked at random and the investigator was blinded
310 to genotypes and treatments. All data from a single experiment, incorporating all 4 experimental
311 groups, was averaged. The number of mice evaluated is indicated in figure legends, with three to
312 four litters examined per experiment.

313 **Statistical Analysis**. All data analyzed followed normal distribution according to the
314 Kolmogorov-Smirnov test. Statistical significance was determined using two-way ANOVA
315 followed by Bonferroni's post hoc test for multiple comparisons. Data analysis was performed
316 using GraphPad Prism and presented as means ± s.e.m.

317 All experiments in this study were blinded and randomized. All mice bred for the
318 experiments were utilized for preplanned experiments and randomized to experimental groups.
319 Visibly sick animals were excluded before data collection and analysis. Data were collected,
320 processed and analyzed randomly. The experimental design, treatments and handling of mice
321 were identical across experiments. Littermates were used as controls with multiple litters (3-4)
322 examined per experiments. All mice (including the MRI study) were bred in the Case Western
323 Reserve Animal Core.

324 **Results:**

325 **Pharmacological Normalization of ERK Activity with an ERK Pathway Inhibitor in**
326 **16p11.2del Mice.**

327 In order to test our hypothesis that there are ERK-mediated pathologic processes
328 occurring in the *16p11.2del* mice, we took advantage of two recently developed brain penetrant

peptides, RB1/RB3, which act in concert to attenuate Ras-ERK activity in the brain(Papale et al., 2016, 2017). These brain penetrant peptides exhibit IC50 values in the micromolar range (Papale et al., 2016). Importantly, these peptides have been successfully used *in vivo* for early post-natal developmental treatments, manifesting a remarkable high degree of tolerability and low toxicity. Based on these promising results, we treated with the RB1/RB3 mix (hereafter termed 'ERK Inhibitor') the pregnant *16p11.2del* carrier dams for 5 consecutive days starting at E10.5, encompassing a critical period of cortical neurogenesis. We observed that the enhanced ERK activity in dorsomedial cortex of *16p11.2del* mice at E14.5 was normalized in the inhibitor-treated mice (Fig. 1a,b,c). At E14.5 two-way ANOVA analysis of ERK1 activity showed a significant effect with respect to genotype ($F[1,59]=21.7$, $p<0.0001$) and inhibitor treatment ($F[1,59]=10.12$, $p=0.002$), but with an interaction between both variables ($F[1,59]=4.05$, $p=0.049$). Bonferonni post-hoc analysis showed a 2-fold increase in ERK1 activity ($p<0.0001$) in the vehicle treated *16p11.2del* mice compared to vehicle treated WT mice that normalized to WT levels following inhibitor treatment. Similarly, ERK2 activity was also significantly affected by both genotype ($F[1,77]=4.31$, $p=0.041$) and inhibitor treatment ($F[1,77]=6.76$, $p=0.011$) when analyzed by two-way ANOVA, however a significant interaction between genotype and drug treatment was present ($F[1,77]=5.08$, $p=0.027$). A Bonferonni post-hoc analysis showed a 49% ($p=0.017$) increase in ERK2 activity in the vehicle treated *16p11.2del* mice compared to vehicle treated WT mice that normalized to WT levels with inhibitor treatment. Importantly, total ERK1 levels were reduced in the *16p11.2del* mice in both vehicle and inhibitor treated animals, with a significant genotype effect observed by two-way ANOVA ($p<0.0001$). We observed significant interactions between the inhibitor and genotype because, interestingly, the dose of the ERK inhibitor (10 mg/kg, i.p.) used in our studies did not alter ERK activity in the WT littermates. In

addition, when ERK1/2 activity was analyzed in P10 embryonically treated mice (Fig. 1d,e), there was an inhibitor effect (pERK1:p=0.005, pERK2:p=0.017) by two-way ANOVA, with a Bonferonni post-hoc analysis showing a 75% ($p<0.01$) and 62% ($p<0.01$) increase in ERK1 and ERK2, respectively, in the *16p11.2del* vehicle treated mice that normalized to WT levels. Thus, a prenatal treatment of embryonic mice resulted in abrogation of abnormal ERK hyperactivity in the developing cortex when examined at E14.5 (Fig. 1b,c) or postnatally at P10 (Fig. 1d, e).

ERK Inhibitor Treatment Rescues Embryonic and Postnatal Cortical Defects in the *16p11.2del* Mice.

Next, we investigated whether the embryonic treatment with the ERK pathway inhibitor could correct aberrant progenitor proliferation dynamics in the developing cortex (Fig. 2 a-b) and rescue deficits in cortical neurogenesis (Fig. 2c-d). We evaluated the number of proliferating, BrdU+ progenitors following a single, 30 min IP BrdU injection at E14.5. A 2-way ANOVA analysis showed no genotype or inhibitor effect, but Bonferroni post-hoc analysis showed a 30% increase ($p<0.05$) in BrdU+ progenitors in the vehicle treated *16p11.2del* mice compared to vehicle treated WT mice. This increase in progenitor proliferation was abrogated in ERK inhibitor treated *16p11.2del* mice and returned to WT levels (Fig.2a). Furthermore, western blot analysis and immunohistochemistry (IHC) demonstrate that the number of Tbr2+ intermediate progenitor cells (IPCs) residing in the SVZ can be restored to normal levels after the inhibitor treatment (Fig. 2b). Western blot analysis of Tbr2 by two-way ANOVA showed a genotype and inhibitor interaction, but post-hoc analysis revealed a 30% decrease in Tbr2 levels ($p<0.0001$) in the vehicle *16p11.2del* mice, which returned to normal following treatment, when compared to vehicle WT mice. This correlated with a 37% decrease (post-hoc Bonferroni, $p=0.0012$) in the

number of Tbr2+ cells by IHC in the vehicle treated *16p11.2del* mice, that corrected to WT levels in the inhibitor treated mice when compared to vehicle WT animals (2-way ANOVA showed significant inhibitor and genotype interaction). Additionally, using western analysis and IHC we also show that treatment with ERK inhibitor ameliorates the aberrant elevation of the number of early born cortical neurons marked by Ctip2+ and Tbr1+ that populate cortical layer V and VI, respectively (Fig.2c-d). Again 2-way ANOVA analyses of IHC and western blots of Tbr1 and Ctip2 showed interactions between genotype and inhibitor, but the post-hoc Bonferroni analysis showed a 50% increase in Ctip2 levels ($p=0.012$) and a 30% increase in Ctip2+ cells by IHC ($p=0.0005$) in the *16p11.2del* vehicle treated mice, which returned to WT levels when compared to WT vehicle treated animals. Tbr1 analysis showed a 35% increased in Tbr1 protein levels ($p=0.038$), and a 20% increase in Tbr1+ cells via IHC ($p=0.025$) in the *16p11.2del* vehicle treated mice that returned to WT levels in the inhibitor treated mice, when compared to WT vehicle treated animals.

Next, we tested whether prenatal ERK inhibitor treatment resulted in permanent rescue of cortical cytoarchitecture defects by evaluation of postnatal mice at P2. We show that the number of Brn1+ and Satb2+ layer II-III pyramidal neurons is restored to normal levels after prenatal ERK inhibitor treatment (Fig.3a-b). These are cortico-cortical connections, some of which project to contralateral hemisphere across the corpus callosum (O'Rourke et al., 1995). Satb2 analysis shows significant genotype ($p=0.048$) and treatment effect ($p=0.013$) by 2-way ANOVA. Post-hoc analysis shows significant 13% reduction in Satb2+ cells in vehicle deletion animals compared to WT vehicle ($p=0.03$), which is abrogated with inhibitor treatment of deletion animals, which show Satb2+ cells similar to vehicle WT animals and significant increase when compared to vehicle treated *16p11.2del* mice ($p=0.01$). Brn1 analysis shows no

genotype or treatment effect by 2-way ANOVA, but post-hoc analysis shows decrease Brn1+ cells in vehicle treated *16p11.2del* mice compared to WT vehicle-treated animals ($p<0.05$), but inhibitor treated *16p11.2del* mice show no difference in Brn1+ cells compared to WT vehicle-treated animals.

Analysis of Tbr1 cells by 2-way ANOVA showed an interaction between genotype and inhibitor treatment, but post-hoc analysis of vehicle treated *16p11.2del* animals showed a 25% increase in Tbr1+ cells compared to vehicle treated WT animals (post-hoc Bonferroni, $p=0.0075$), which is rescued with treatment of *16p11.2del* animals with ERK inhibitor (Fig. 3d), consistent with the effect of the inhibitor on these neurons observed at E14.5 (Fig.2d). The number of Ctip2+ layer V neurons, known to project to sub-cortical targets including the thalamus, midbrain, pons and spinal cord, is increased during mid-neurogenesis, but decreased postnatally in vehicle 16p11.2del mice when compared to WT vehicle treated mice (post-hoc Bonferroni, $p =0.014$) and normalized by inhibitor treatment of *16p11.2del* animals, which have more Ctip2+ neurons compared to vehicle *16p11.2del* animals ($p=0.033$) and no difference compared to WT vehicle treated animals (Fig.2c, 3c). It is unknown why these projection neurons are ultimately lost in the *16p11.2del* mice. These data demonstrate the developmental rescue of cortical deficits in progenitor proliferation and neurogenesis in the *16p11.2del* after pharmacological intervention with the ERK pathway inhibitor.

ERK inhibitor treatment normalizes levels of the cell cycle regulators p27 ^{Kip1} and cyclin D1.

To examine whether the aberrant generation of cortical neurons is due to deficits in cell cycle dynamics, we examined two critical cell cycle regulators: p27 ^{Kip1} and cyclin D1 (Fig.4),

which are directly regulated by ERK signaling and play an important role in progenitor proliferation (Calegari and Huttner, 2003; Dehay and Kennedy, 2007; Lange et al., 2009; Pucilowska et al., 2012). We performed IHC and western blot analysis and observed a significant decrease in $p27^{Kip1}$ protein levels in the *16p11.2del* cortex, consistent with our previous observations. Two-way ANOVA analysis of $p27^{kip1}$ showed no genotype or inhibitor effect, but post-hoc analysis showed a 31% decrease ($p<0.01$) in $p27^{kip1}$ levels in the 16p11.2del vehicle treated mice compared to the WT vehicle treated animals, which normalized to 92% of the vehicle WT level after inhibitor treatment (Fig. 4b'-b"). When cyclin D1 levels were analyzed by two-way ANOVA, there was only a inhibitor effect ($F[1,46], p<0.0001$), but no genotype effect, with significant decrease in cyclin D1 in the inhibitor treated *16p11.2del* mice ($p<0.001$) compared to the vehicle treated *16p11.2del* mice (Fig.4a-a"). These data show that the *16p11.2del* mice exhibit ERK dependent changes in cell-cycle dynamics of neural progenitor cells that are ameliorated with the prenatal ERK inhibitor treatment.

ERK inhibitor treatment partially rescues hippocampal and septal morphoanatomical abnormalities in *16p11.2del* mice

To determine whether ERK inhibitor treatment would affect macroscale brain morphoanatomy in *16p11.2del* mice, we applied voxelwise Tensor Based Morphometry (TBM) and automated anatomical labeling to high-resolution MRI brain scans (Pagani et al., 2016). Consistent with previous reports (Horev et al., 2011), *16p11.del* mice showed increases in the relative volume of the hypothalamus, superior colliculus and periaqueductal grey when compared to control (WT) mice (Fig. 5a). Voxelwise TBM mapping also revealed foci of decreased volume in ventral hippocampal, amygdalar, entorhinal and lateral septal areas in

444 *16p11.2del* mice when compared to WT controls (Fig.5a). Importantly, treatment with the ERK
445 inhibitor partially-rescued ventral hippocampal and lateral septal volume in *16p11.2del* mice
446 when compared to vehicle treated controls (Fig. 5b-c). Interestingly, the ventral hippocampus is
447 a region where pERK is highly expressed during mid-neurogenesis and a key substrate for
448 anxiety-related behavior (Kjelstrup et al., 2002; Maren and Holt, 2004) which these mice exhibit.
449
450 **Rescue of behavioral deficits in *16p11.2del* mice after prenatal ERK inhibitor treatment.**
451 We, as well as others, have previously shown that the 16p11.2del mice are smaller than
452 their WT littermates (Horev et al., 2011; Portmann et al., 2014; Pucilowska et al., 2015; Tidyman
453 and Rauen, 2016). We report that prenatal treatment with ERK pathway inhibitor restored
454 normal body weight in the *16p11.2del* mice when examined at 3 months of age (WT vehicle
455 treated: 35.015g; *16p11.2del* vehicle treated: 25.352g; *16p11.2del* inhibitor-treated: 29.396g).
456 The *16p11.2 del* mice are reported to exhibit many behavioral deficits (Horev et al.,
457 2011; Portmann et al., 2014; Pucilowska et al., 2015; Yang et al., 2015). We tested the
458 *16p11.2del* and WT control mice in a number of standard behavioral paradigms that are altered
459 by the *16p11.2* deletion. Specifically, we assayed open field to evaluate hyperactivity and
460 anxiety-like behaviors, novel object and fear conditioning to examine hippocampal dependent
461 memory, elevated-plus maze (EPM) to test anxiety as well as maternal behavior and olfaction.
462 We evaluated three large cohorts (n=30/genotype) of 3 month-old male mice (except for
463 maternal behavior and olfaction). Data was analyzed by 2-way ANOVA, but unless otherwise
464 indicated, significant interaction occurred between the genotype and inhibitor treatment, which
465 resulted in reliance on post-hoc analysis to show genotype or inhibitor effects.
466 We first conducted the EMP test, where examining entries into the closed arm, the post-

hoc analysis showed fewer closed arm entries by vehicle *16p11.2del* mice compared to vehicle WT mice ($p<0.05$), which was rescued in the inhibitor treated deletion animals who showed more closed arm entries compared to vehicle treated *16p11.2del* animals ($p<0.05$) and no difference with vehicle treated WT animals. Furthermore, we observed statistical significance in time spent in the open arm ($p<0.05$), which was only partially rescued by inhibitor treatment with no genotype or inhibitor effect by 2-way ANOVA. We also noted an increase in open arm immobility, indicating freezing behavior (6a). In the open field test (Fig. 6b), we first examined level of activity which showed that the *16p11.2del* mice did not explore the field as much as the WT mice. 2-way ANOVA analysis of total distance travelled showed significant genotype ($F[1,76]$, $p=0.005$) and drug effect ($F[1,76]$, $p=0.02$) with no interaction, although post-hoc tests did not show significance between vehicle WT and *16p11.2del* animals or vehicle and inhibitor treated *16p11.2del* animals. However, in the open field test (Fig. 6b), we observed that vehicle treated *16p11.2del* mice spent more time in the center compared to vehicle treated WT mice (post-hoc Bonferroni, $p<0.01$), which was rescued by ERK inhibitor treatment, as inhibitor treated *16p11.2del* mice were similar to vehicle treated WT mice and spent less time in the center compared to the vehicle treated *16p11.2del* mice (post-hoc Bonferroni, $p<0.05$). Interestingly, total distance travelled was also increased in the vehicle treated *16p11.2del* mice compared to vehicle treated WT mice (post-hoc Bonferroni, $p<0.05$), which again normalized with inhibitor treatment of *16p11.2del* mice, who showed significant decreased in distance travelled compared to vehicle treated *16p11.2del* n animals ($p<0.05$) and no difference with vehicle treated WT animals.

Contextual fear conditioning showed significantly higher freezing percentage in the vehicle treated *16p11.2del* mice compared to the vehicle treated WT cohort (post-hoc

Bonferroni, $p<0.01$) indicating impaired contextual memory (Fig. 6c). This is improved by treatment of the *16p11.2del* animals with the ERK inhibitor, which show no difference compared to vehicle treated WT animals, but no significant difference was observed between vehicle and inhibitor treated *16p11.2del* animals.

Novel object recognition (NOR) did not reveal a significant genotype or inhibitor effect in post-hoc analysis, but a trend showing impaired NOR in vehicle treated *16p11.2del* compared to vehicle treated WT mice ($p=0.16$), which improved with inhibitor treatment of *16p11.2del* mice, who showed a trend toward improvement in NOR compared to vehicle treated *16p11.2del* mice ($p=0.11$) (Fig 6d).

Both male and female *16p11.2del* mice exhibited a significantly higher acuity in their sense of smell compared to the WT mice (post-hoc Bonferroni, $p<0.01$), which was attenuated after the treatment (Fig 6f). Inhibitor treated *16p11.2del* mice showed significant attenuation in olfaction compared to vehicle treated *16p11.2del* mice ($p<0.0001$).

Additionally, females showed heightened maternal response, as measured in a pup retrieval assay that was reduced following ERK inhibitor treatment (Fig. 6e). Vehicle treated *16p11.2del* animals showed decreased latencies to retrieving all pups compared to vehicle treated WT animals (pup1: $p<0.01$, pup2: $p<0.01$, pup3: $p<0.001$). This effect was reverted with treatment of *16p11.2del* animals with inhibitor as no difference in latencies was observed when compared to WT vehicle treated animals (post-hoc Bonferroni, $p<0.01$).

Altogether, the above evidence supports the notion that an early pharmacological intervention targeting ERK signaling in *16p11.2del* mice is sufficient to reverse some of the behavioral alterations found in this model of ASD.

Postnatal treatment with ERK inhibitor partially restores behavioral deficits of adult *16p11.2del* mice.

We next questioned whether any of the behavioral deficits could be improved by ERK inhibitor treatment in adult mice. Therefore, we treated 3 month-old WT and *16p11.2del* male mice with ERK inhibitor for 5 consecutive days at P90.

In the elevated plus maze, we observed that vehicle treated *16p11.2del* animals spent more time in the open arm compare to the vehicle WT cohort (Fig. 7a; post-hoc Bonferroni, $p < 0.05$). This effect was abrogated in ERK inhibitor treated *16p11.2del* animals as no difference in open arm time was observed when compared to vehicle treated WT animals (2-way ANOVA showed significant interaction between genotype and inhibitor treatment). In the open field test, we did not observe significant genotype effects between vehicle treated *16p11.2del* and WT animals in post-hoc analysis, however, we did observe a trend toward more open entries in vehicle *16p11.2 del* animals compared to WT (Fig. 7b). In addition, treatment of *16p11.2del* animals with the ERK inhibitor showed significant reduction in entries into the center of the field compared to vehicle treated *16p11.2del* animals (post-hoc Bonferroni, $p<0.01$). Although the adult treated mice did not achieve statistical significance in the olfactory test, there was a trend toward heightened acuity in the *16p11.2del* mice, which was at least partially recovered after the inhibitor treatment (Fig. 7d). Together our data suggests that post-natal treatment with the ERK inhibitor may result in partial rescue of some of the behavioral deficits seen in the *16p11.2del* mice.

Since other models linked to ASDs and the ERK pathway show aberrant levels of oxytocin (Hollander et al., 2007), we examined 3 month-old male mice and show that levels of oxytocin are elevated in the *16p11.2del* male mice and importantly can be restored to normal

after inhibitor treatment (post-hoc Bonferroni, $p<0.01$)(Fig.7c). We observed by 2-way ANOVA a significant genotype ($F(1, 24) = 6.132$, p0.0207) and drug effect ($F(1, 24) = 8.712$, $p=0.0070$) and significant interaction $F(1, 24) = 4.884$, $p=0.0369$.

The *16p11.2del* mice do not exhibit typical social deficits that are common among other models of ASDs as well as *16p11.2del* patients, thus, the enhanced oxytocin levels, which normally augment social interactions, could be masking the social impairment in these mice. Further studies using oxytocin inhibitors could clarify this phenomenon.

Discussion:

ERK/MAPK pathway as a potential target for ASD therapy

The ERK/MAPK pathway has been extensively studied and found to play pivotal roles in neural development as well as in learning, memory, synaptic plasticity and spine dynamics (Thomas and Huganir, 2004). The functional importance of signaling through this pathway is also reflected in the effects of activating mutations that alter the activity of the ERK1/2 kinases and result in a constellation of syndromic and non syndromic neurodevelopmental disorders, including the RASopathies and the associated intellectual disability (Tidyman and Rauen, 2016; Borrie et al., 2017).

It has recently been appreciated that some forms of ASD are also associated with perturbations of several intracellular signaling cascades, including the Ras-ERK and the mTORC1 pathways (Kalkman, 2012; Adviento et al., 2014; Borrie et al., 2017). In addition to genetic linkages, pathway network analyses point to a convergence of a wide range of abnormalities associated with autism onto a few salient pathways, prominent amongst these is the ERK/MAPK pathway (Wen et al., 2016; Mitra et al., 2017). Importantly, many ASD mouse models with genetic alterations of Mecp2, FMR1, NF1, Syngap as well as, BTBR and

559 *16p11.2del* exhibit aberrant ERK signaling (Liang et al., 2010; Osterweil et al., 2010, 2013;
560 Hamdan et al., 2011; Bhakar et al., 2012; Wang et al., 2013; Golzio et al., 2012; Kelleher III et
561 al., 2012; Wang et al., 2012; Faridar et al., 2014; Pucilowska et al., 2015). These data argue that
562 the abnormal ERK activity in the brain is central to pathology of many ASDs.
563 We and others have previously shown that the genetic deletion of the *16p11.2* interval
564 results in a paradoxical increase in ERK activity that is associated with aberrant neural
565 progenitor proliferation which leads to dysregulation in the number of neurons generated within
566 the cortex (Pucilowska et al., 2015) and subcortical structures (Portmann et al., 2014; Grissom et
567 al., 2018). This results in altered volumes of the cortical lamina and subcortical nuclei.
568 These studies raise the possibility that ERK inhibitors can be used to normalize their
569 activity and have therapeutic efficacy in *16p11.2* deletion carriers. We reasoned that
570 normalization of ERK activity might rescue the CNS phenotypes observed in the *16p11.2del*
571 mice. It is noteworthy that Papale et al., utilizing the newly developed ERK pathway inhibitor
572 peptides, have recently shown that the treatment ameliorates defective synaptogenesis in a
573 genetic model of RASopathy (Papale et al., 2017). Moreover, they have shown its effectiveness
574 of ERK pathway inhibition by treatment of murine models of cocaine addiction, suppressing the
575 behavioral phenotypes (Papale et al., 2016).

576 *ERK inhibitor suppresses the increase in ERK activity in 16p11.2del mice*
577 The *16p11.2del* mice exhibit paradoxical increase in ERK activity in both the developing
578 and mature brain. This finding was unexpected given that the deletion removes the *Mapk3* gene
579 encoding ERK1. The biological basis of dysregulation of the ERK pathway in this model is
580 unknown. However, we and others have previously postulated that ERK1 acts a negative
581 regulator of ERK2 (Mazzucchelli et al., 2002; Vantaggiato et al., 2006; Fasano and Brambilla,

582 2011; Trabalzini and Retta, 2014) and our findings are consistent with this hypothesis but basis
583 of the elevated ERK1 activity remains unclear. We found that basal ERK activity in wildtype
584 mice was not altered by drug treatment and this likely represents the intrinsic basal activity of the
585 ERKs that is independent of upstream regulators, and thus not subject to further inhibition by the
586 RB1 peptide.

587 The *16p11.2* deletion contains 27 genes. Mice lacking ERK1or ERK2 do not recapitulate
588 the entire range of defects observed in the *16p11.2del* mice, implicating the contribution of other
589 genes within this interval to the ASD phenotypes. Importantly, at least two other genes (*MVP*
590 and *KCTD13*) within the deleted region converge onto the MAPK pathway and affect cell
591 proliferation, mGluR5 signaling and protein turnover (Liang et al., 2010; Golzio et al., 2012;
592 Tian et al., 2015). This suggests that multiple genes within the deletion interval converge on the
593 ERK/MAPK pathway resulting in an overall increase in ERK activity.

594

595 *ERK inhibitor rescues cortical defects in 16p11.2del mice*

596 We provide mechanism-based evidence showing that treatment with ERK inhibitors
597 during the peak of neurogenesis rescues the structural and behavioral deficits observed in the
598 *16p11.2del* mice. Specifically, we found that the aberrant generation of cortical neurons was
599 restored to normal levels owing to normalization of neurogenesis following developmental drug
600 treatment. This was secondary to the ERK- dependent modulation of potent cell cycle regulators
601 cyclin D1 and $p27^{Kip1}$. The retention of normal numbers of neural progenitors during critical
602 neurogenic period allowed for generation of appropriate numbers of cells populating cortical
603 lamina as well as normal circuitry. Importantly, we corraborated our molecular and biochemical
604 findings with MRI data showing partial reversal of volumetric changes to the ventral

hippocampus and lateral septum. It is of interest to note that the MRI analyses showed that the ERK inhibitor treatment did not rescue all of the anatomical abnormalities in the brain, which may be related to a short treatment window implemented in this study and the temporal variation in neurogenesis between different brain regions.

ERK Inhibitor rescues behavioral deficits in 16p11.2del mice

One of the most striking findings from this study is the reversal of a wide range of behavioral deficits that arise from the *16p11.2* deletion. Our data shows the first developmental rescue of ASD associated phenotypes in the *16p11.2del* mouse model. The data from the elevated plus maze and open field did show statistical significance for changes in anxiety-like behaviors but not as strong as in previous studies, which is possibly due to increased sample size, longer handling habituation period and greater statistical rigor. However, we do observe significant improvement in contextual fear memories in the inhibitor treated *16p11.2del* mice. It is conceivable that the observed ventral hippocampal morphological rescue could explain the inhibitor effect on anxiety-like behaviors and contextual memory, given the established roles of these brain regions in emotional and stress coping responses (Kjelstrup et al., 2002; Bannerman et al., 2003; Maren and Holt, 2004; Adhikari et al., 2011).

The strongest effects we found were in olfaction and maternal behaviors, where we observed heightened responses in *16p11.2del* mice, which were attenuated with inhibitor treatment. The decrease in latencies to retrieve pups and locate hidden food in the deletion mice may represent enhanced sensory perception or processing, but may also reflect changes to neural circuitry that govern motivational behavior.

Remarkably, we also report a partial rescue of the behavioral deficits by inhibitor treatment of adult mice. This effect is likely due to the fact that ERK dysregulation persists into

adulthood in the *16p11.2del* animals (Pucilowska et al., 2015) and potentially disrupts the normal role of ERK signaling in synaptic plasticity. At the synapse ERKs promote regulation of translational mechanisms promoting protein synthesis and thus cognition (Thomas and Huganir, 2004). These synaptic changes ultimately lead to refinement of neuronal connectivity. Furthermore, many mutations associated with ASDs converge on the ERK pathway impairing cognitive functioning and adaptive behavioral plasticity (Komiyama et al., 2002; Levitt and Campbell, 2009; Ebert and Greenberg, 2013). Correcting hyperactive ERK signaling in the adult *16p11.2del* mice may thus lead to ameliorating of behavioral phenotypes that are mediated by the post-natal functions of ERK signaling. Importantly, these data suggest that dysregulation of ERK activity can be rescued during brain development through restoration of normal cortical proliferation dynamics, and in adult mice, presumably due to the synaptic actions of the ERKs previously described in this mouse model (Tian et al., 2015; Lu et al., 2018).

We show that normalization of ERK signaling in the *16p11.2del* mice can reverse the molecular and behavioral phenotypes in the *16p11.2del* mice. While we observe significant effects on neuronal population sizes, our analysis was restricted to cortical neurons and, given that this is a germline hemideletion model, other areas of the nervous system are undoubtedly affected. This is further supported by our imaging analysis that shows multiple brain regions that are affected by the deletion. While we observe some behavioral improvements from post-natal treatment with the ERK/MAPK inhibitor, further analysis of changes to neuronal morphology and synaptic physiology in the *16p11.2del* mice is warranted to help characterize the post-natal effects of the *16p11.2* deletion. Finally, we have only examined a few behavioral phenotypes and gender differences in behaviors were not examined.

In conclusion, our findings lead to three important conclusions. Our data strongly

supports the hypothesis that ASDs are neurodevelopmental disorders affecting global brain circuitry. Secondly, our work significantly strengthens the emerging hypothesis that multiple disorders of impaired cognition and ASDs converge onto a few fundamental pathways, such as the ERK/MAPK pathway, and affect a critical period of brain development. Finally, the cognitive and neuropsychiatric symptoms of *16p11.2* microdeletion disorder are amenable to targeted drug therapy, both during development and in the adult.

References:

Adhikari A, Topiwala MA, Gordon JA (2011) Single units in the medial prefrontal cortex with anxiety-related firing patterns are preferentially influenced by ventral hippocampal activity. Neuron 71:898–910 .

Adviento B, Corbin IL, Widjaja F, Desachy G, Enrique N, Rosser T, Risi S, Marco EJ, Hendren RL, Bearden CE, Rauen KA, Weiss LA (2014) Autism traits in the RASopathies. J Med Genet 51:10–20.

Avants BB, Tustison N, Song G (2009) Advanced normalization tools (ANTS). Insight J 2:1–35.

Bannerman DM, Grubb M, Deacon RMJ, Yee BK, Feldon J, Rawlins JNP (2003) Ventral hippocampal lesions affect anxiety but not spatial learning. Behav Brain Res 139:197–213.

Bhakar AL, Dölen G, Bear MF (2012) The Pathophysiology of Fragile X (and What It Teaches Us about Synapses). Annu Rev Neurosci 35:417–443.

Borrie SC, Brems H, Legius E, Bagni C (2017) Cognitive Dysfunctions in intellectual disabilities: The contributions of the Ras-MAPK and PI3K-AKT-mTOR pathways. Annu Rev Genomics Hum Genet 18:115–142.

Calegari F, Huttner WB (2003) An inhibition of cyclin-dependent kinases that lengthens, but does not arrest, neuroepithelial cell cycle induces premature neurogenesis. J Cell Sci 116:4947–4955.

Cutuli D, Pagani M, Caporali P, Galbusera A, Laricchiuta D, Foti F, Neri C, Spalletta G, Caltagirone C, Petrosini L, Gozzi A (2016) Effects of Omega-3 fatty acid supplementation on cognitive functions and neural substrates: A voxel-based morphometry study in aged mice. Front Aging Neurosci 8:38-52.

Dehay C, Kennedy H (2007) Cell-cycle control and cortical development. Nat Rev Neurosci 8:438–450.

Dorr AE, Lerch JP, Spring S, Kabani N, Henkelman RM (2008) High resolution three-dimensional brain atlas using an average magnetic resonance image of 40 adult C57Bl/6J mice. Neuroimage 42:60–69.

Ebert DH, Greenberg ME (2013) Activity-dependent neuronal signalling and autism spectrum disorder. Nature 493:327–337.

688 Faridar A, Jones-Davis D, Rider E, Li J, Gobius I, Morcom L, Richards LJ, Sen S, Sherr EH
689 (2014) Mapk/Erk activation in an animal model of social deficits shows a possible link to
690 autism. Mol Autism 5:57.
691 Fasano S, Brambilla R (2011) Ras-ERK Signaling in Behavior: Old Questions and New
692 Perspectives. Front Behav Neurosci 5:79.
693 Freedman TS, Sondermann H, Friedland GD, Kortemme T, Bar-Sagi D, Marqusee S, Kuriyan J
694 (2006) A Ras-induced conformational switch in the Ras activator Son of sevenless. Proc
695 Natl Acad Sci 103:16692–16697.
696 Ghebranious N, Giampietro PF, Wesbrook FP, Rezkalla SH (2007) A novel microdeletion at
697 16p11.2 harbors candidate genes for aortic valve development, seizure disorder, and mild
698 mental retardation. Am J Med Genet A 143A:1462–1471.
699 Glickstein SB, Monaghan JA, Koeller HB, Jones TK, Ross ME (2009) Cyclin D2 Is Critical for
700 Intermediate Progenitor Cell Proliferation in the Embryonic Cortex. J Neurosci 29:9614–
701 9624.
702 Golzio C, Willer J, Talkowski ME, Oh EC, Taniguchi Y, Jacquemont S, Reymond A, Sun M,
703 Sawa A, Gusella JF, Kamiya A, Beckmann JS, Katsanis N (2012) KCTD13 is a major
704 driver of mirrored neuroanatomical phenotypes of the 16p11.2 copy number variant. Nature
705 485:363–367.
706 Grissom NM, McKee SE, Schoch H, Bowman N, Havekes R, O'Brien WT, Mahrt E, Siegel S,
707 Commons K, Portfors C, Nickl-Jockschat T, Reyes TM, Abel T (2018) Male-specific
708 deficits in natural reward learning in a mouse model of neurodevelopmental disorders. Mol
709 Psychiatry 23:544–555.
710 Hamdan FF, Daoud H, Piton A, Gauthier J, Dobrzeniecka S, Krebs M-O, Joober R, Lacaille J-C,
711 Nadeau A, Milunsky JM, Wang Z, Carmant L, Mottron L, Beauchamp MH, Rouleau GA,
712 Michaud JL (2011) De Novo SYNGAP1 Mutations in Nonsyndromic Intellectual Disability
713 and Autism. Biol Psychiatry 69:898–901.
714 Hanson E et al. (2015b) The cognitive and behavioral phenotype of the 16p11.2 deletion in a
715 clinically ascertained population. Biol Psychiatry 77:785–793.
716 Hollander E, Bartz J, Chaplin W, Phillips A, Sumner J, Soorya L, Anagnostou E, Wasserman S
717 (2007) Oxytocin increases retention of social cognition in autism. Biol Psychiatry 61:498–
718 503.
719 Horev G, Ellegood J, Lerch JP, Son Y-EE, Muthuswamy L, Vogel H, Krieger AM, Buja A,
720 Henkelman RM, Wigler M, Mills AA (2011) Dosage-dependent phenotypes in models of
721 16p11.2 lesions found in autism. Proc Natl Acad Sci 108:17076–17081.
722 Kalkman HO (2012) Potential opposite roles of the extracellular signal-regulated kinase (ERK)
723 pathway in autism spectrum and bipolar disorders. Neurosci Biobehav Rev 36:2206–2213.
724 Kelleher III RJ, Geigenmüller U, Hovhannisyan H, Trautman E, Pinard R, Rathmell B,
725 Carpenter R, Margulies D (2012) High-Throughput Sequencing of mGluR Signaling
726 Pathway Genes Reveals Enrichment of Rare Variants in Autism Esteban FJ, ed. PLoS One
727 7:e35003.
728 Kjelstrup KG, Tuvnes FA, Steffenach H-A, Murison R, Moser EI, Moser M-B (2002) Reduced
729 fear expression after lesions of the ventral hippocampus. Proc Natl Acad Sci U S A
730 99:10825–10830.
731 Komiyama NH, Watabe AM, Carlisle HJ, Porter K, Charlesworth P, Monti J, Strathdee DJC,
732 O'Carroll CM, Martin SJ, Morris RGM, O'Dell TJ, Grant SGN (2002) SynGAP regulates
733 ERK/MAPK signaling, synaptic plasticity, and learning in the complex with postsynaptic

734 density 95 and NMDA receptor. J Neurosci 22:9721–9732.
735 Kumar RA, KaraMohamed S, Sudi J, Conrad DF, Brune C, Badner JA, Gilliam TC, Nowak NJ,
736 Cook EH, Dobyns WB, Christian SL (2007) Recurrent 16p11.2 microdeletions in autism.
737 Hum Mol Genet 17:628–638.
738 Lange C, Huttner WB, Calegari F (2009) Cdk4/CyclinD1 Overexpression in neural stem cells
739 shortens G1, delays neurogenesis, and promotes the generation and expansion of basal
740 progenitors. Cell Stem Cell 5:320–331.
741 Levitt P, Campbell DB (2009) The genetic and neurobiologic compass points toward common
742 signaling dysfunctions in autism spectrum disorders. J Clin Invest 119:747–754.
743 Levy D, Ronemus M, Yamrom B, Lee Y, Leotta A, Kendall J, Marks S, Lakshmi B, Pai D, Ye
744 K, Buja A, Krieger A, Yoon S, Troge J, Rodgers L, Iossifov I, Wigler M (2011) Rare De
745 Novo and Transmitted Copy-Number Variation in Autistic Spectrum Disorders. Neuron
746 70:886–897.
747 Liang P, Wan Y, Yan Y, Wang Y, Luo N, Deng Y, Fan X, Zhou J, Li Y, Wang Z, Yuan W, Tang
748 M, Mo X, Wu X (2010) MVP interacts with YPEL4 and inhibits YPEL4-mediated activities
749 of the ERK signal pathway. Biochem Cell Biol 88:445–450.
750 Liu S, Sun J-P, Zhou B, Zhang Z-Y (2006) Structural basis of docking interactions between
751 ERK2 and MAP kinase phosphatase 3. Proc Natl Acad Sci 103:5326–5331.
752 Lu H-C, Mills AA, Tian D (2018) Altered synaptic transmission and maturation of hippocampal
753 CA1 neurons in a mouse model of human chr16p11.2 microdeletion. J Neurophysiol
754 119:1005–1018.
755 Maren S, Holt WG (2004) Hippocampus and Pavlovian fear conditioning in rats: muscimol
756 infusions into the ventral, but not dorsal, hippocampus impair the acquisition of conditional
757 freezing to an auditory conditional stimulus. Behav Neurosci 118:97–110.
758 Marshall CR et al. (2008) Structural variation of chromosomes in autism spectrum disorder. Am
759 J Hum Genet 82:477–488.
760 Mazzucchelli C et al. (2002) Knockout of ERK1 MAP kinase enhances synaptic plasticity in the
761 striatum and facilitates striatal-mediated learning and memory. Neuron 34:807–820.
762 Mitra I, Lavillaureix A, Yeh E, Traglia M, Tsang K, Bearden CE, Rauen KA, Weiss LA (2017)
763 Reverse Pathway Genetic Approach Identifies Epistasis in Autism Spectrum Disorders Flint
764 J, ed. PLOS Genet 13:e1006516.
765 Newbern J, Zhong J, Wickramasinghe RS, Li X, Wu Y, Samuels I, Cherosky N, Karlo JC,
766 O'Loughlin B, Wikenheiser J, Gargesha M, Doughman YQ, Charron J, Ginty DD,
767 Watanabe M, Saitta SC, Snider WD, Landreth GE (2008) Mouse and human phenotypes
768 indicate a critical conserved role for ERK2 signaling in neural crest development. Proc Natl
769 Acad Sci 105:17115–17120.
770 O'Rourke NA, Sullivan DP, Kaznowski CE, Jacobs AA, McConnell SK (1995) Tangential
771 migration of neurons in the developing cerebral cortex. Development 121:2165–2176.
772 Osterweil EK, Chuang S-C, Chubykin AA, Sidorov M, Bianchi R, Wong RKS, Bear MF (2013)
773 Lovastatin corrects excess protein synthesis and prevents epileptogenesis in a mouse model
774 of fragile X syndrome. Neuron 77:243–250.
775 Osterweil EK, Krueger DD, Reinhold K, Bear MF (2010) Hypersensitivity to mGluR5 and
776 ERK1/2 leads to excessive protein synthesis in the hippocampus of a mouse model of
777 fragile X syndrome. J Neurosci 30:15616–15627.
778 Pagani M, Damiano M, Galbusera A, Tsaftaris SA, Gozzi A (2016) Semi-automated registration-
779 based anatomical labelling, voxel based morphometry and cortical thickness mapping of the

mouse brain. J Neurosci Methods 267:62–73.
Papale A, d'Isa R, Menna E, Cerovic M, Solari N, Hardingham N, Cambiaghi M, Cursi M, Barbacid M, Leocani L, Fasano S, Matteoli M, Brambilla R (2017) Severe intellectual disability and enhanced gamma-aminobutyric acidergic synaptogenesis in a novel model of rare RASopathies. Biol Psychiatry 81:179–192.
Papale A, Morella IM, Indrigo MT, Bernardi RE, Marrone L, Marchisella F, Brancale A, Spanagel R, Brambilla R, Fasano S (2016) Impairment of cocaine-mediated behaviours in mice by clinically relevant Ras-ERK inhibitors. Elife 5. pii: e17111.
Portmann T et al. (2014) Behavioral abnormalities and circuit defects in the basal ganglia of a mouse model of 16p11.2 deletion syndrome. Cell Rep 7:1077–1092.
Pucilowska J, Puzerey PA, Karlo JC, Galan RF, Landreth GE (2012) Disrupted ERK Signaling during Cortical Development Leads to Abnormal Progenitor Proliferation, Neuronal and Network Excitability and Behavior, Modeling Human Neuro-Cardio-Facial-Cutaneous and Related Syndromes. J Neurosci 32:8663–8677.
Pucilowska J, Vithayathil J, Tavares EJ, Kelly C, Karlo JC, Landreth GE (2015) The 16p11.2 Deletion Mouse Model of Autism Exhibits Altered Cortical Progenitor Proliferation and Brain Cytoarchitecture Linked to the ERK MAPK Pathway. J Neurosci 35:3190–3200.
Roskoski R (2012) ERK1/2 MAP kinases: Structure, function, and regulation. Pharmacol Res 66:105–143.
Sondermann H, Soisson SM, Boykevisch S, Yang S-S, Bar-Sagi D, Kuriyan J (2004) Structural analysis of autoinhibition in the ras activator Son of Sevenless. Cell 119:393–405.
Sweatt JD (2004) Mitogen-activated protein kinases in synaptic plasticity and memory. Curr Opin Neurobiol 14:311–317.
Thomas GM, Huganir RL (2004) MAPK cascade signalling and synaptic plasticity. Nat Rev Neurosci 5:173–183.
Tian D, Stoppel LJ, Heynen AJ, Lindemann L, Jaeschke G, Mills AA, Bear MF (2015) Contribution of mGluR5 to pathophysiology in a mouse model of human chromosome 16p11.2 microdeletion. Nat Neurosci 18:182–184.
Tidyman WE, Rauen KA (2009) The RASopathies: developmental syndromes of Ras/MAPK pathway dysregulation. Curr Opin Genet Dev 19:230–236.
Tidyman WE, Rauen KA (2016) Pathogenetics of the RASopathies. Hum Mol Genet 25:R123–R132.
Trabalzini L, Retta SF (2014) Ras signaling: methods and protocols. New York: Humana Press.
Ullmann JFP, Watson C, Janke AL, Kurniawan ND, Reutens DC (2013) A segmentation protocol and MRI atlas of the C57BL/6J mouse neocortex. Neuroimage 78:196–203.
Vantaggiato C, Formentini I, Bondanza A, Bonini C, Naldini L, Brambilla R (2006) ERK1 and ERK2 mitogen-activated protein kinases affect Ras-dependent cell signaling differentially. J Biol 5(5):14.
Wang C-C, Held RG, Hall BJ (2013) SynGAP regulates protein synthesis and homeostatic synaptic plasticity in developing cortical networks PLoS One 8:e83941.
Wang Y, Kim E, Wang X, Novitch BG, Yoshikawa K, Chang L-S, Zhu Y (2012) ERK inhibition rescues defects in fate specification of Nf1-deficient neural progenitors and brain abnormalities. Cell 150:816-830..
Wen Y, Alshikho MJ, Herbert MR (2016) Pathway network analyses for autism reveal multisystem involvement, major overlaps with other diseases and convergence upon MAPK and calcium signaling. PLoS One 11:e0153329.

826 Worsley KJ, Evans AC, Marrett S, Neelin P (1992) A Three-Dimensional Statistical Analysis for
827 CBF Activation Studies in Human Brain. J Cereb Blood Flow Metab 12:900–918.
828 Yang M, Mahrt EJ, Lewis F, Foley G, Portmann T, Dolmetsch RE, Portfors C V., Crawley JN
829 (2015) 16p11.2 Deletion Syndrome Mice Display Sensory and Ultrasonic Vocalization
830 Deficits During Social Interactions. Autism Res 8:507–521.
831 Zufferey F et al. (2012) A 600 kb deletion syndrome at 16p11.2 leads to energy imbalance and
832 neuropsychiatric disorders. J Med Genet 49:660–668.
833
834
835
836
837
838
839
840
841
842
843
844
845
846
847
848
849
850
851
852

Figure Legends:

Fig. 1 Rescue of ERK activity with an ERK pathway inhibitor in *16p11.2del* mice at E14.5 and P10. **a)** IHC of E14.5 coronal sections from mice treated with vehicle (veh) or ERK inhibitor (inh). Veh treated *16p11.2del* mice shows upregulation of ERK activity in the dorsomedial cortex * (anti-pERK; green). This is abrogated after 5 days of inhibitor treatment starting at E10.5. **(b)** Western analysis of E14.5 veh or inh treated cortical lysates. **(c)** Quantification of Western analysis showing a significant increase in ERK1 and ERK2 activity in *16p11.2del* animals (pERK1, ****p<0.0001 and pERK2, *p<0.05), which is restored to normal level after inhibitor treatment (## p=0.0087; # p<0.05) (veh.treated: nWT = 19, nDel=13; inh.treated: nWT = 19, nDel=12). ERK1 total levels are decreased in vehicle deletion animals (**p<0.01) and inhibitor animals (****p<0.0001) (veh.treated: nWT = 8, nDel=7; inh.treated: nWT = 10, nDel=9) **(d)** Western analysis of P10 veh or inh treated cortical lysates **(e)** Western analysis of P10 veh or inh prenatally treated cortical lysates, quantified in (e) ERK1 and ERK2 activity are elevated in deletion animals at P10 (pERK1 **p<0.01; pERK2, p**<0.01), which is normalized in embryonic inhibitor treatment (#p<0.05, ###p<0.001). All values normalized to loading control GAPDH or CoxIV and reported as a fold change. P values are from Bonferroni post-hoc analysis (* compares WT to deletion, # compares vehicle deletion to inhibitor deletion).

Fig. 2 Reversal of deficits in cortical neurogenesis in the *16p11.2del* mice after treatment with ERK pathway inhibitor at E14.5. Immunohistochemistry (IHC) of coronal sections and western analyses of cortical lysates at E14.5 (a) IHC with proliferation marker, BrdU injected 30 min. prior to sacrifice. (a') The number of BrdU+ progenitors was analyzed (veh.treated: nWT = 8, nDel=6; inh.treated: nWT = 9, nDel=9); (*p<0.05, #p<0.05) . (b) IHC with intermediate

progenitor marker, Tbr2 (green). (b') Quantification of Tbr2+ progenitors (veh. treated: nWT = 11, nDel=4; inh.treated: nWT = 9, nDel=16) (**p<0.0012, ##p<0.0052). (b") Quantification of western analysis (veh.treated: nWT = 29, nDel=37; inh.treated: nWT = 23, nDel=21), (****p<0.00001, #p<0.0388). (c) IHC for layer V marker, Ctip2 (red). (c') Quantification of Ctip2+ neurons (veh. treated: nWT = 5, nDel=4; inh. treated: nWT = 4, nDel=6)(***p=0.0005, ####p<0.0001, *p=0.026). (c") Quantification of western analysis (veh treated: nWT=15, nDel=9; inh treated nWT= 8, nDel=11), (*p=0.0186, ##p=0.0073). (d) IHC with layer VI marker, Tbr1 (green). (d') Quantification of Tbr1+ neurons (veh.treated: nWT = 9, nDel=9; inh.treated: nWT = 5, nDel=5) (*p=0.025, ###p=0.0004). (d") Quantification of Western analysis (veh. treated: nWT=15, nDel=7; inh treated: nWT= 11, nDel=12) (*p=0.038, ##p=0.0017). All western analyses data represented as a fold change, normalized to a loading control. P values are from Bonferroni post-hoc analysis (* compares WT to deletion, # compares vehicle deletion to inhibitor deletion).

Fig. 3 Prenatal treatment with an ERK pathway inhibitor stably restores normal cortical cytoarchitecture *16p11.2del* mice. (a) Mice were evaluated at P2 by IHC with layer II-IV marker Brn1, (green). (a') Quantification of Brn1+ neurons shows a rescue in somatosensory cortex of *16p11.2del* mice (veh treated: nWT=11, nDel=13; inh treated: nWT= 17, nDel=17) (*p<0.05). (b) IHC with layer 2-4 marker, Satb2 (red). (b') Quantification of Satb2+ neurons. (veh treated: nWT=14, nDel=13; inh treated: nWT= 10, nDel=15) (*p=0.033, #p=0.0105). (c) IHC with layer V marker, Ctip2 (red). (c') Quantification of Ctip2+ neurons (veh treated: nWT=21, nDel=14; inh treated: nWT= 9, nDel=13) (*p=0.014, #p=0.033). (d) IHC with layer VI marker, Tbr1+ (green). (d') Quantification of Tbr1+ neurons (veh treated: nWT=8, nDel=9; inh

900 treated: nWT= 12, nDel=10) (**p=0.0076, #p=0.0535). P values are from Bonferroni post-hoc
901 analysis (* compares WT to deletion, # compares vehicle deletion to inhibitor deletion).
902
903 **Fig. 4 Treatment with ERK pathway inhibitor normalizes the levels of the downstream**
904 **ERK effectors: p27 ^{Kip1} and cyclin D1.** IHC of coronal sections and western analyses from WT
905 and *16p11.2del* mice at E14.5 (a) Immunostaining against CyclingD1 antibody (green), (a')
906 Western blot analysis, quantified in (a") (veh treated: nWT=16, nDel=7; inh treated: nWT=16,
907 nDel=13) (***p<0.001); (b) Immunostaining against p27^{Kip1}(green), (b') Western blot analysis,
908 quantified in (b") (veh treated: nWT=8, nDel=10; inh treated: nWT=8, nDel=10) (**p<0.01,
909 *p<0.05). P values are from Bonferroni post-hoc analysis.
910
911 **Fig. 5 Prenatal ERK inhibitor treatment partially rescues ventral hippocampal and**
912 **lateral septal volume in 16p11.2del mice.** Mice were treated for 5 consecutive days starting
913 at E10.5 and evaluated at P90. **(a)** TBM analyses revealed significant increased volume of SC,
914 PAG and Hypo in *16p11.2del* mice compared to WT littermates (*t*-test, $p < 0.01$ FWE cluster-
915 corrected, with cluster defining threshold of $|t| > 2.3$). In *16p11.2* deletion mice, we also
916 observed an increased volume of the RS ctx, as well as reduced volume of vHPC, LS, Ent ctx
917 and Amy (t-test, $p < 0.01$ FWE cluster-corrected, with cluster defining threshold of $|t| > 2.3$). **(b)**
918 Comparison between treated and non-treated *16p11.2del* mice shows that ERK-inhibitor
919 produces bilateral foci of increased volume in the vHPC and LS (t-test, $p < 0.01$ FWE cluster-
920 corrected, with cluster defining threshold of $|t| > 2.3$). (c) A composite illustration of panels (a)
921 and (b) revealed that foci of increased gray matter volume (red/yellow, from panel b) are
922 spatially located in the same hippocampal and septal regions exhibiting reduced gray matter

volume in 16p11.2 del mice (blu/light blue, from panel a), suggesting a partial anatomical rescue of volumetric deficits upon treatment with ERK inhibitor. **(d-e)** Consistent with TBM results, anatomical labelling revealed reduced relative volume in vHPC (t-test: $t_{17} = 3.78$, $p = 0.001$) and LS (t-test: $t_{17} = 2.21$, $p = 0.041$) in *16p11.2del* mice compared to WT littermates (one-way ANOVA of vHPC: $F_{3,34} = 8.083$, $p < 0.001$; one-way ANOVA of LS: $F_{3,34} = 1.692$, $p = 0.1872$). Treatment with ERK inhibitor in *16p11.2del* mice partially restored morphoanatomical volume in these brain regions (vHPC, t-test: $t_{16} = 2.79$, $p = 0.013$), although the effects in LS did not reach full statistical significance (t-test, $t_{16} = 1.78$, $p = 0.078$). Amy, amygdala; Ent ctx, entorhinal cortex; Hypo, hypothalamus; LS, lateral septum; PAG, periaqueductal grey; RS, retrosplenial cortex; SC, superior colliculus; vHPC, ventral hippocampus. *p<0.05,**p<0.01.

Fig. 6 Reversal of Behavioral Impairment of *16p11.2del* mice after prenatal ERK pathway inhibitor treatment. WT or 16p11.2del -months old male or female mice treated with Veh or Inh at E10.5 for 5 days. (a) Elevated plus maze shows a no change in percentage of time in open arm, but decreased closed arm time in 16p11.2del mice that is rescued by inhibitor treatment (*p<0.05, #p<0.05) (veh treated: nWT=25, nDel=22; inh treated: nWT=27, nDel=28); (b) Open Field shows increased time spent in center in 16p11.2del mice that is rescued with inhibitor treatment (**p<0.01, #p<0.05) (veh treated: nWT=23, nDel=20; inh treated: nWT=19, nDel=18). (c) Fear conditioning shows increased freezing in 16p11.2del animals that improves with inhibitor treatment (**p<0.01) (veh treated: nWT=5, nDel=6; inh treated: nWT=11, nDel=11), cond. stimulus: 85 dB sound at 2800 Hz for 30 sec.; unconditioned stimulus (US: 0.56mA). Retention test performed 18 hrs later for 5 minutes in the absence of tone; (d) NOR was evaluated in WT and 16p11.2del animals (#p<0.05) (veh treated: nWT=16, nDel=12; inh treated: nWT=8, nDel=16); (e) Naïve females were exposed to 3 WT pups placed in 3 corner of the cage,

time to retrieve pups was recorded, (1st pup: **p<0.01; 2nd pup: **p<0.01; 3rd pup: ***p=0.001) (veh treated: nWT=21, nDel=17; inh treated: nWT=6, nDel=6). (f) Mice were food deprived for 24 hours, then placed in a cage containing one food pellet (teddy graham) buried under normal cage bedding, time to retrieve was recorded (**p<0.01, ####p<0.0001) (veh treated: nWT=22, nDel=22; inh treated: nWT=22, nDel=7). P values are from Bonferroni post-hoc analysis (* compares WT to deletion, # compares vehicle deletion to inhibitor deletion).

Fig. 7 Postnatal treatment with ERK pathway inhibitor partially restores behavioral deficits in adult *16p11.2del* mice. WT or *16p11.2del* 3-months old male or female mice treated with Veh or Inh at P90 for 5 days. (a) Elevated plus maze analysis of percentage of time in open arm (*p<0.05), entries in open arm, immobility time (##p<0.01) and total distance traveled (veh treated: nWT=15, nDel=11; inh treated: nWT=12, nDel=7); (b) Open Field analysis of entries into center (##p<0.01), time spent in center and total distance traveled (veh treated: nWT=22, nDel=17; inh treated: nWT=23, nDel=9). (c) ELISA performed on whole brain lystaed of P90 mice (** p<0.05; #p<0.05) (veh treated: nWT=10, nDel=8; inh treated: nWT=7, nDel=5). (d) Mice were food deprived for 24 hours, then placed in a cage containing one food pellet (teddy graham) buried under normal cage bedding, time to retrieve (latency) was analyzed. P values are from Bonferroni post-hoc analysis (* compares WT to deletion, # compares vehicle deletion to inhibitor deletion).

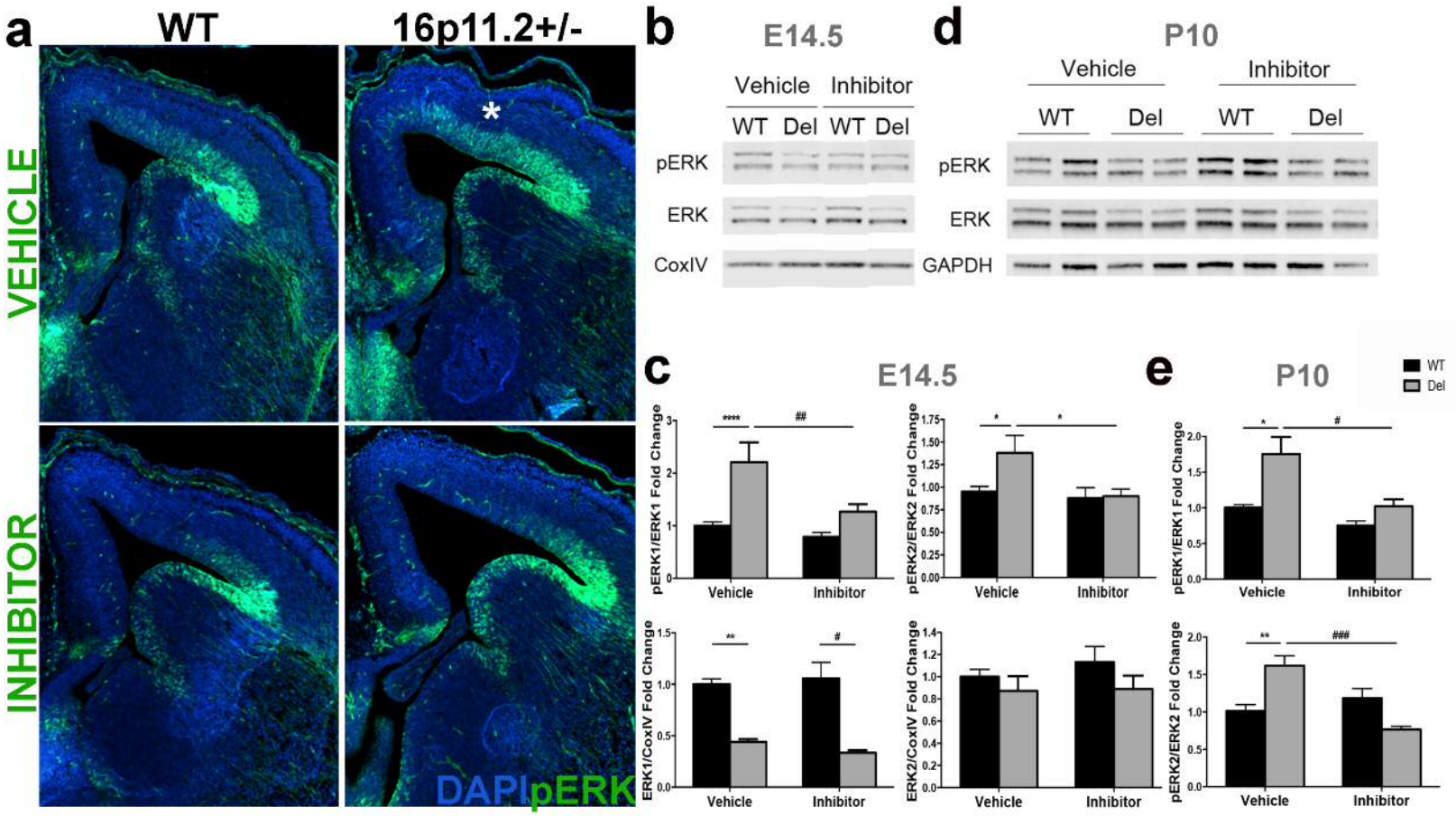
a
WT
16p11.2+/-
VEHICLE
INHIBITOR
*
DAPIpERK
b
E14.5
Vehicle
Inhibitor
WT
Del
WT
Del
pERK
ERK
CoxIV
d
P10
Vehicle
Inhibitor
WT
Del
WT
Del
pERK
ERK
GAPDH
c
E14.5
pERK1/ERK1 Fold Change
pERK2/ERK2 Fold Change
ERK1/CoxIV Fold Change
ERK2/CoxIV Fold Change
Vehicle
Inhibitor
e
P10
WT
Del
pERK1/ERK1 Fold Change
pERK2/ERK2 Fold Change
Vehicle
Inhibitor

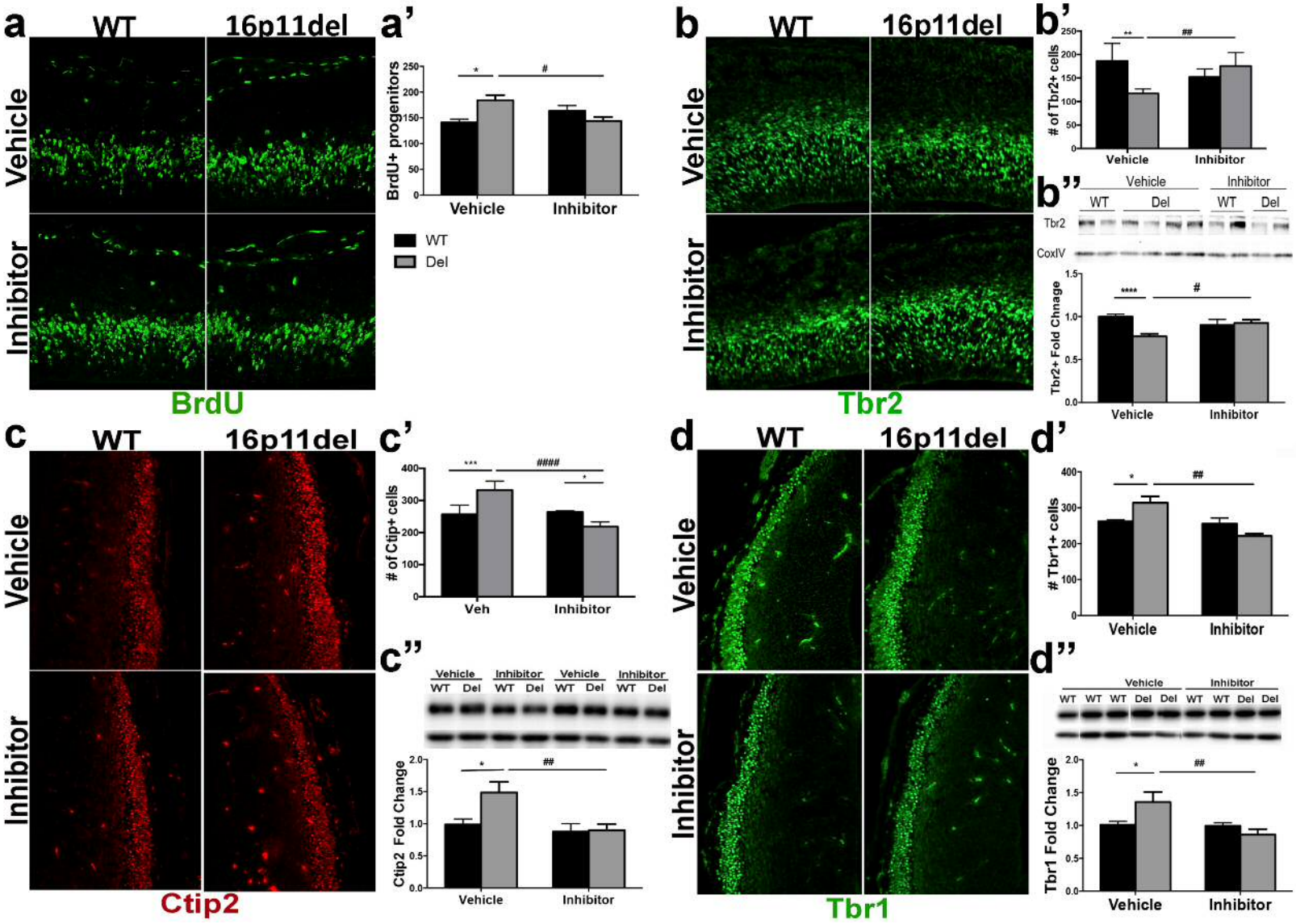
a
WT
16p11del
Vehicle
Inhibitor
BrdU
a'
BrdU+ progenitors
Vehicle
Inhibitor
WT
Del
b
WT
16p11del
Vehicle
Inhibitor
Tbr2
b'
# of Tbr2+ cells
Vehicle
Inhibitor
b''
Vehicle
Inhibitor
WT
Del
WT
Del
Tbr2
CoxIV
Tbr2+ Fold Chnage
Vehicle
Inhibitor
c
WT
16p11del
Vehicle
Inhibitor
Ctip2
c'
# of Ctip+ cells
Veh
Inhibitor
c''
Vehicle
Inhibitor
Vehicle
Inhibitor
WT
Del
WT
Del
WT
Del
WT
Del
Ctip2 Fold Change
Vehicle
Inhibitor
d
WT
16p11del
Vehicle
Inhibitor
Tbr1
d'
Tbr1+ cells
Vehicle
Inhibitor
d''
Vehicle
Inhibitor
WT
WT
WT
Del
Del
WT
WT
Del
Del
Tbr1 Fold Change
Vehicle
Inhibitor

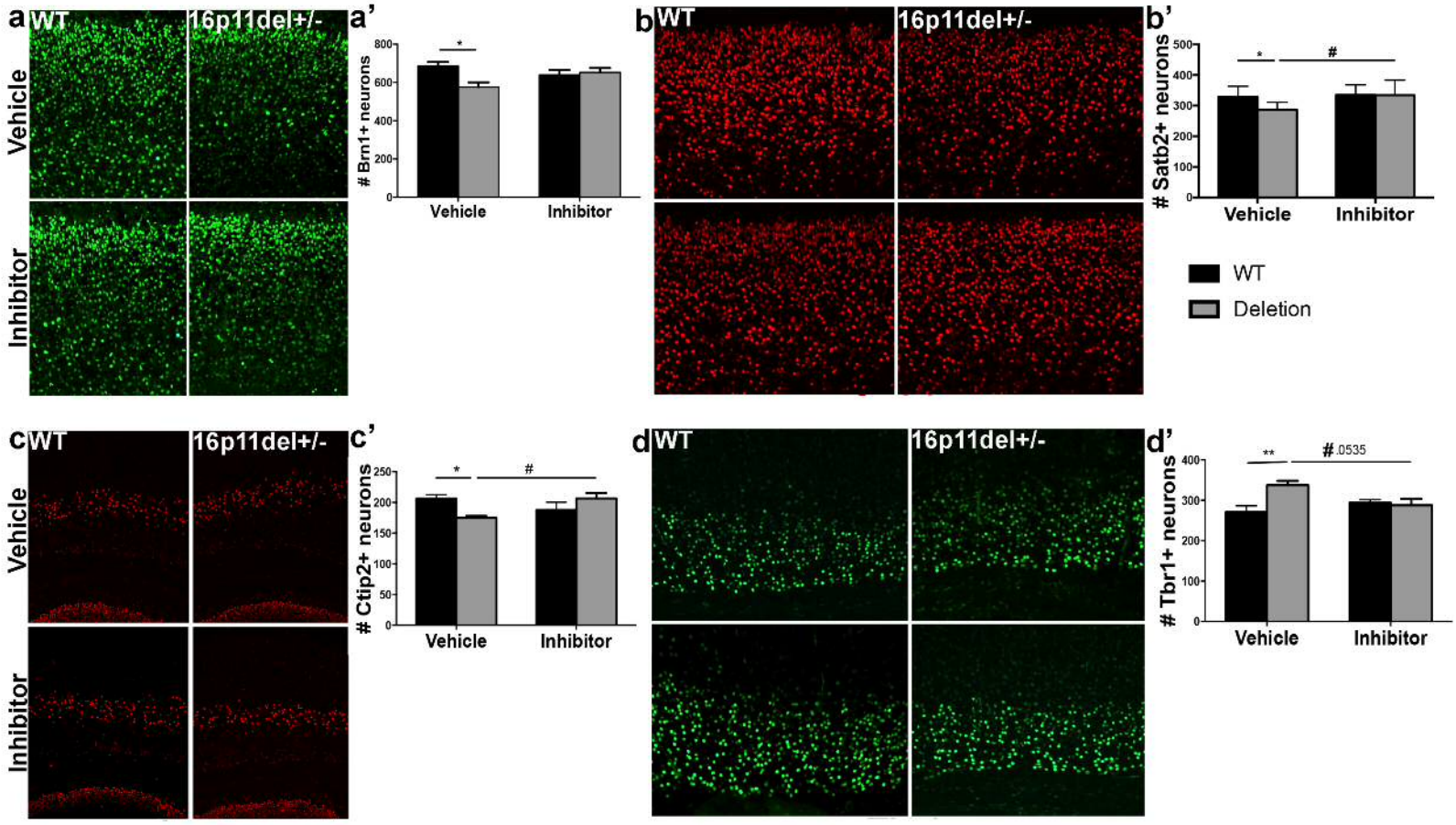
a
WT
16p11del+/-
Vehicle
Inhibitor
a'
Brn1+ neurons
800
600
400
200
0
*
Vehicle
Inhibitor
b
WT
16p11del+/-
b'
Satb2+ neurons
500
400
300
200
100
0
*
#
Vehicle
Inhibitor
WT
Deletion
c
WT
16p11del+/-
Vehicle
Inhibitor
c'
Ctip2+ neurons
250
200
150
100
50
0
*
#
Vehicle
Inhibitor
d
WT
16p11del+/-
d'
Tbr1+ neurons
400
300
200
100
0
**
#.0535
Vehicle
Inhibitor

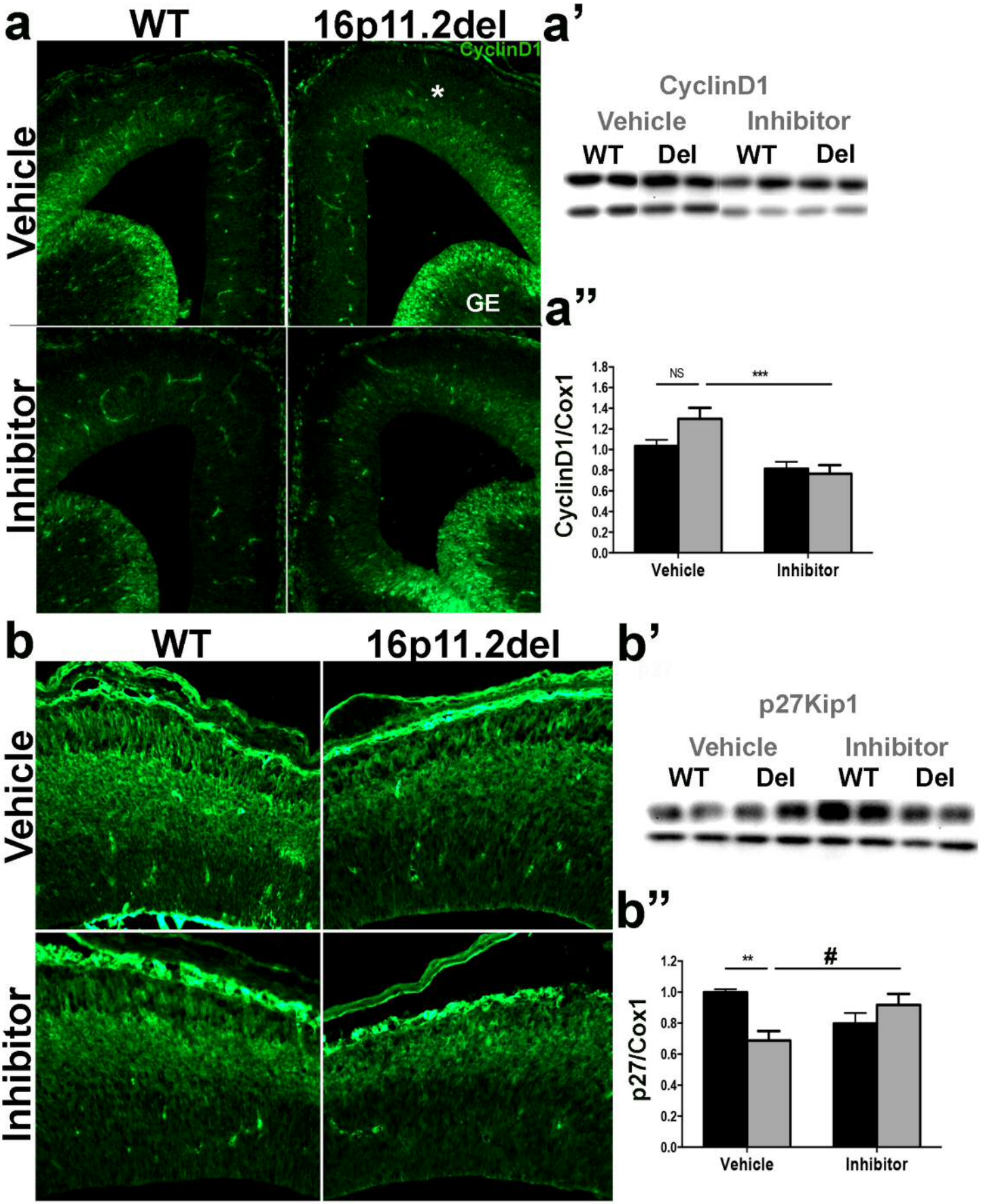
a
WT
16p11.2del
a'
CyclinD1
Vehicle
Inhibitor
*
GE
a''
CyclinD1
Vehicle
Inhibitor
WT
Del
WT
Del
CyclinD1/Cox1
NS
***
1.8
1.6
1.4
1.2
1.0
0.8
0.6
0.4
0.2
0.0
Vehicle
Inhibitor
b
WT
16p11.2del
b'
p27Kip1
Vehicle
Inhibitor
WT
Del
WT
Del
b''
p27/Cox1
**
#
1.2
1.0
0.8
0.6
0.4
0.2
0.0
Vehicle
Inhibitor

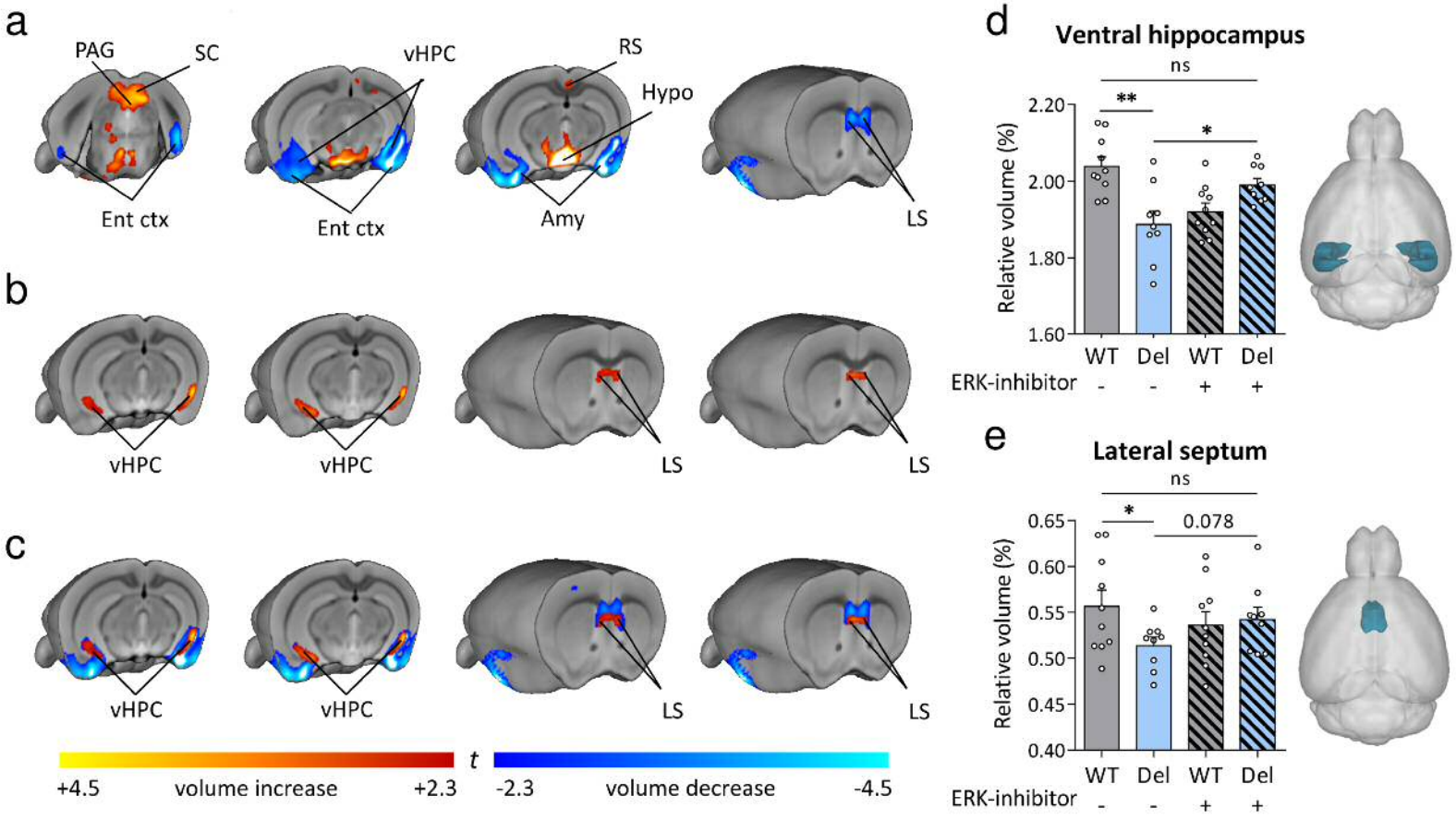
a
PAG
SC
Ent ctx
vHPC
Ent ctx
RS
Hypo
Amy
LS
b
vHPC
vHPC
LS
LS
c
vHPC
vHPC
LS
LS
t
+4.5
volume increase
+2.3
-2.3
volume decrease
-4.5
d
Ventral hippocampus
ns
**
*
Relative volume (%)
2.20
2.00
1.80
1.60
WT
Del
WT
Del
ERK-inhibitor
-
-
+
+
e
Lateral septum
ns
*
0.078
Relative volume (%)
0.65
0.60
0.55
0.50
0.45
0.40
WT
Del
WT
Del
ERK-inhibitor
-
-
+
+

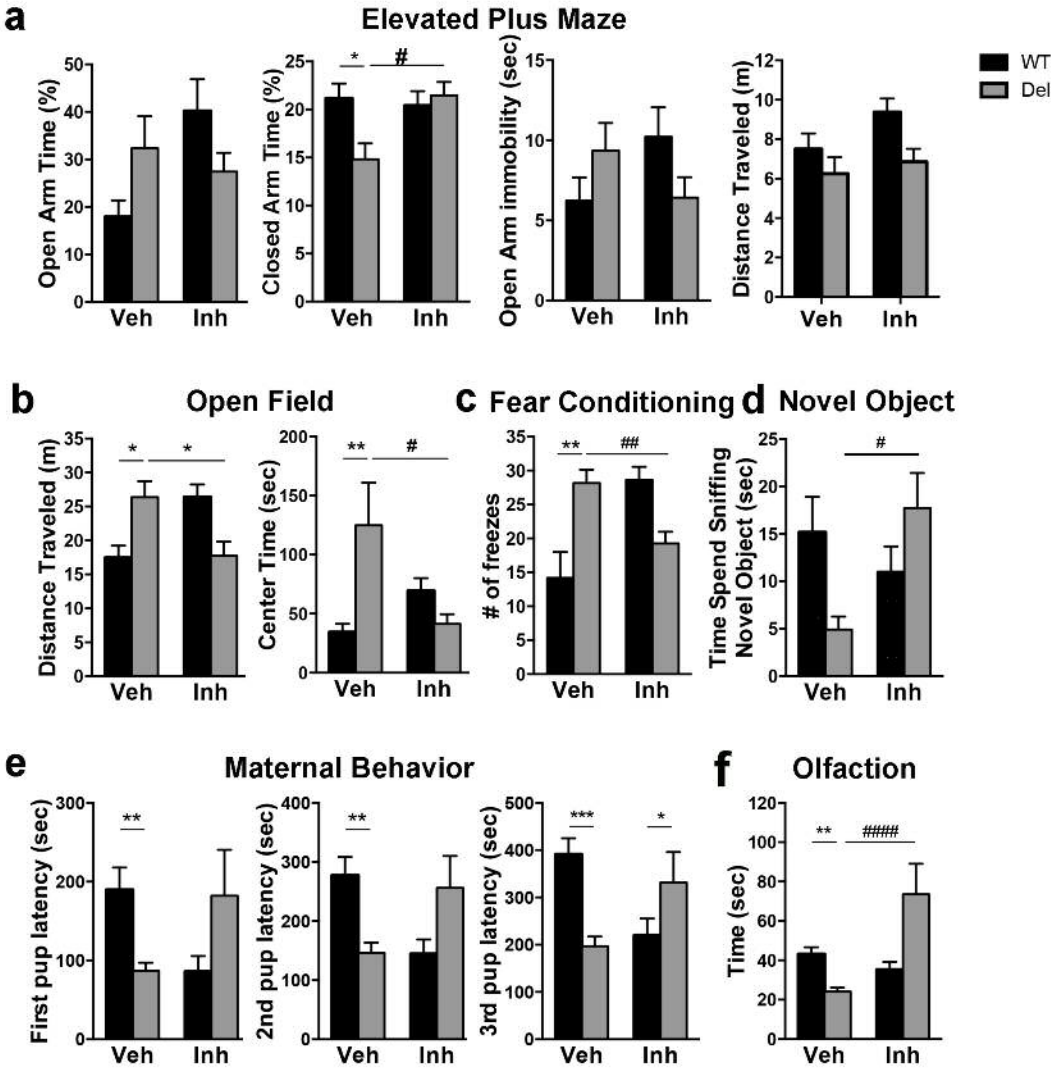
a
Elevated Plus Maze
WT
Del
Open Arm Time (%)
Closed Arm Time (%)
Open Arm immobility (sec)
Distance Traveled (m)
Veh
Inh
b
Open Field
Distance Traveled (m)
Center Time (sec)
c
Fear Conditioning
# of freezes
d
Novel Object
Time Spend Sniffing Novel Object (sec)
e
Maternal Behavior
First pup latency (sec)
2nd pup latency (sec)
3rd pup latency (sec)
f
Olfaction
Time (sec)

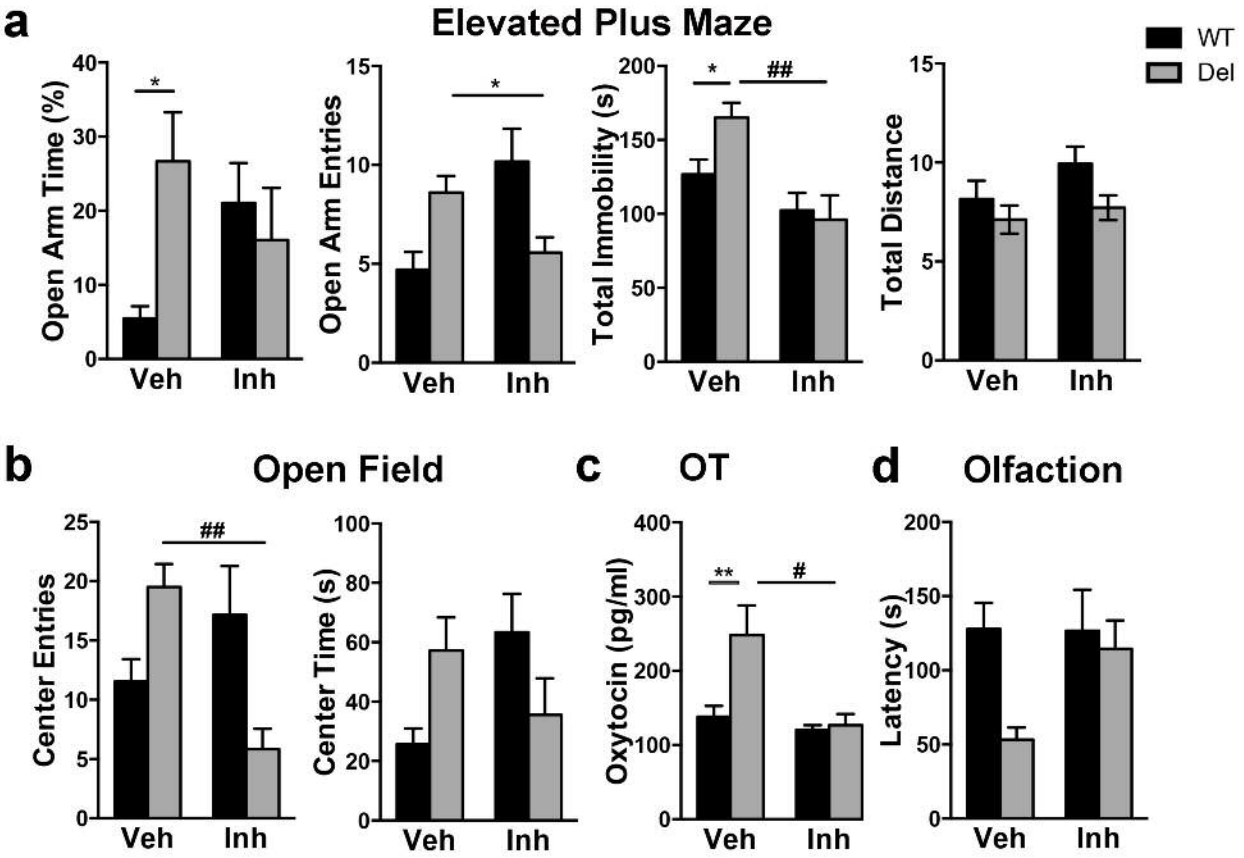
a
Elevated Plus Maze
WT
Del
Open Arm Time (%)
Open Arm Entries
Total Immobility (s)
Total Distance
Veh
Inh
b
Open Field
Center Entries
Center Time (s)
c
OT
Oxytocin (pg/ml)
d
Olfaction
Latency (s)